Solutions for Transients in Arbitrarily Branching Cables: II. Voltage Clamp Theory

Guy Major, Jonathan D. Evans, and J. Julian B. Jack
University Laboratory of Physiology, Oxford, OX1 3PT, United Kingdom

ABSTRACT Analytical solutions are derived for arbitrarily branching passive neurone models with a soma and somatic shunt, for synaptic inputs and somatic voltage commands, for both perfect and imperfect somatic voltage clamp. The solutions are infinite exponential series. Perfect clamp decouples different dendritic trees at the soma: each exponential component exists only in one tree; its time constant is independent of stimulating and recording position within the tree; its amplitude is the product of a factor constant over that entire tree and factors dependent on stimulating and recording positions. Imperfect clamp to zero is mathematically equivalent to voltage recording with a shunt. As the series resistance increases, different dendritic trees become more strongly coupled. A number of interesting response symmetries are evident. The solutions reveal parameter dependencies, including an insensitivity of the early parts of the responses to specific membrane resistivity and somatic shunt, and an approximately linear dependence of the slower time constants on series resistance, for small series resistances. The solutions are illustrated using a "cartoon" representation of a CA1 pyramidal cell and a two-cylinder + soma model.

INTRODUCTION

In the previous accompanying paper (1), which will be referred to as "I" below, a separation of variables solution was derived for voltage transients in a passive cable model of an arbitrarily branching neurone with a soma and a somatic shunt. The solution (I.56)[1] is an infinite series of exponentially decaying components, with time constants τ_n (I.24), which hold over the entire cell, and depend on eigenvalues α_n which are the roots of a recursive transcendental equation (I.22). The amplitude of each component, which was derived using complex residues, is the product of three parts: E_n (I.34), which is a constant over the entire cell, depending on electrical and morphological parameters, and ψ_{en} and ψ_{rn} (I.26), which are continuous functions depending on the input and recording sites, respectively.

The methods of Rall (Ref. 2, section III), Rall and Segev (3), Bluman and Tuckwell (4), Evans et al. (5), and Paper I are extended below to derive analogous solutions for current and voltage transients in an arbitrarily branching geometry under voltage clamp at one point. The solutions are further extended to cover imperfect voltage clamp. Implementations are similar to those in the previous paper. Illustrative examples are given. Further, more practically oriented examples are given in the third paper of this series (6) referred to as "III" below. A number of important biological points are made in Paper III concerning parameter dependencies, and problems with voltage clamp.

Programs for waveform generation and fitting under voltage clamp have been written in ANSI-C, based on the solutions below, and will be supplied on request, together with further implementation details.

Received for publication 22 October 1992 and in final form 26 February 1993.

Address reprint requests to Guy Major at the University of Physiology, Parks Rd., Oxford OX1 3PT, United Kingdom.

0006-3495/93/07/450/19 $2.00

[1] Notation for equations used in this series of three accompanying papers (1, 6). "I.56" refers to Eq. 56 of Paper I.

GLOSSARY AND CONVENTIONS

The conventions and symbols in Paper I, are adhered to throughout (see Paper I, List of Symbols and Table I.1). Frequently repeated additional symbols are listed in Table 1 below. Key equations appear in boxes. $\mathcal{S}(j)$ is the stem segment of segment j and *subtree*(p) is the set consisting of segment p and all its descendants. Earth, resting membrane potential, and the reversal potential for shunts are all taken to be zero.

As in the previous paper (1), the dendritic morphology consists of uniform cylindrical segments, with every segment labeled by an index j. As before, the branching pattern is coded using set notation.

PERFECT VOLTAGE CLAMP

Definition of system

This is as in Paper I, Eqs. I.3–I.7, except that the somatic boundary condition is now

$$V_s = V_{\text{com}}(t), \tag{1}$$

where $V_{\text{com}}(t)$ is the command voltage as a function of time.

We consider the two following basic initial conditions:

(I) Unit charge synaptic impulse

$V_{\text{com}}(t) = 0$ and

$$V_j(X_j, Z_e, 0) = \begin{cases} (\tau_m g_{\infty_e})^{-1} \delta(X_e - Z_e), & \text{if } j = e, \\ 0 & \text{otherwise,} \end{cases} \tag{2}$$

i.e. the command voltage is set to zero, and there is a unit point charge into segment e.

TABLE 1 Additional symbols (to those in Paper I)

$A^{iq}_{n_r}$	nth clamp current amplitude term [nA] from unit dendritic charge, (Eq. 19)
A^{iv}_{n}	nth clamp current amplitude term from unit voltage command impulse, (Eq. 24)
$A^{vq}_{n_{rr}}$	nth voltage amplitude term from unit dendritic point charge, (Eq. 16)
$A^{vv}_{n_r}$	nth voltage amplitude term from unit voltage command impulse, (Eq. 22)
D	constant in spatial part of separation of variables solution [mV] (Eq. 4)
D_n	D when $\alpha = \alpha_n$
$E_{n_{st}}$	part of amplitude term, constant over input tree (zero if this not source tree of α_n) [mV] (Eq. 14)
$i_{\text{clamp}}(Z,t)$	measured clamp current [nA]
i_{syn}	actual synaptic current [nA]
g_{ser}	series conductance ($= 1/R_{\text{ser}}$) [MΩ]
g_{sm}	soma membrane conductance ($= 1/R_{\text{sm}}$) [MΩ]
g_s^*	$g_s + g_{\text{ser}} = g_{\text{sm}} + g_{\text{shunt}} + g_{\text{ser}}$ [nS]
R	ratio of soma membrane resistance to series resistance ($= R_{\text{sm}}/R_{\text{ser}}$)
R_{ss}	input resistance measured at clamp point (Eqs. I.78, 32)
R^*_{ss}	input resistance measured at clamp point, including g_{ser} (Eq. I.78)
R_{ser}	series resistance, imperfect voltage clamp ($= 1/g_{\text{ser}}$) [MΩ]
R_{shunt}	shunt resistance, $= 1/g_{\text{shunt}}$ [MΩ]
R_{sm}	soma membrane resistance ($= 1/g_{\text{sm}} = R_{\text{m}}/a_{\text{s}}$) [GΩ]
$\mathcal{S}(j)$	stem segment of tree containing segment j
$subtree(p)$	set of indices of segment p and all its descendants
t_{1090}	10–90% rise time [ms]
t_{2080}	20–80% rise time [ms]
t_{peak}	time to peak [ms]
$V_{\text{com}}(t)$	command voltage function [mV]
ϵ^*	$c_s/(g_s^*\tau_m)$ [dimensionless]
k_j	continuity factor: $\kappa_{st} = 1$, $\forall st \in stems$ under perfect voltage clamp (Eq. I.28)
$\hat{k}_j$	steady-state continuity factor $= \bar{\kappa}_j$ with $q = 1$
$\hat{\mu}_j$	steady-state branching factor (Eq. 30)
τ_{eff}	effective time constant, e.g., fitted $t_{\text{peak}} + 0.7$ to $t_{\text{peak}} + 20$ ms [ms]

(II) Unit voltage command impulse

$$V_{\text{com}}(t) = \delta(t) \quad \text{and} \quad V_j(X_j, Z_e, 0) = 0 \tag{3}$$

i.e. a unit command voltage impulse at the soma, with no charge impulses into any segment.

Because the system is linear, the solution to an arbitrary voltage command together with an arbitrary pattern of synaptic input can be obtained from the responses to these two cases, by convolution.

Nonsomatic point clamp

Although it is possible to solve the system when one or more special branch points with soma-like lumped capacitances and conductances are included away from the clamp point, the increase in mathematical complexity argues for a different strategy. To achieve nonsomatic clamp, it is easy to modify a given model, by placing a "soma" (with zero conductance) at the clamp point, and by representing the real soma as a short cylindrical segment with the correct surface area, in the appropriate place. Stems, parents, and daughters are reassigned with the new clamp point as the origin. The equation system described above then adequately specifies the model.

Case I: Solution for a unit charge synaptic impulse

As in Paper I, we use the technique of separation of variables to solve the problem (Eqs. I.3–I.7, 2). In the following sections we present the main results only, with the reader being referred to the previous paper for the details. The separable solutions of Eq. I.3 for voltage clamp can still be written as Eq. I.13, where α^2 is the separation constant. The spatial part of the solution $y_j(X_j)$ can be written

$$y_j(X_j) = D\kappa_j[\cos\alpha(L_j - X_j) + \mu_j \sin\alpha(L_j - X_j)], \tag{4}$$

where D, μ_j, and κ_j are arbitrary constants.

Recursive transcendental equation for eigenvalues

Application of the boundary conditions gives the same expressions (Eqs. I.19 and I.20) for the μ_j terms, as in Paper I. Eq. I.28 still holds for the κ_j terms. Unlike in the previous paper, we now have freedom in specifying κ_{st}, since Eq. 4 satisfies Eq. 1 with $V_{\text{com}} = 0$, and for definiteness we prescribe

$$\kappa_{st} = 1 \quad \text{for all stem segments } st. \tag{5}$$

At the soma, the condition (Eq. 1) combined with Eq. 2, gives

$$\cot\alpha L_{st} + \mu_{st} = 0, \quad \text{for all stem segments } st. \tag{6}$$

Eqs. 6 and I.19, together with Eq. I.20, define a recursive transcendental equation, which must be solved to obtain the eigenvalues α_n, $n = 0, 1, 2, 3, \ldots$, of the system, satisfying the boundary conditions and other model parameters. The indexing convention used in Paper I (1) is followed here: n starts from 0. The intention is to make it clear that the slowest time constant under voltage clamp is the limit of τ_0 from the voltage recording solution as g_{shunt} tends to infinity.[2]

A dendritic tree is taken to include one stem segment and all its descendant segments. We note that the voltage clamp decouples the different dendritic trees at the soma (e.g., Ref. 3). This is reflected in Eq. 6: each α_n and the corresponding τ_n (except in the case of repeated roots), is generated by one dendritic tree only, and the corresponding component of the solution exists in that tree only (see below).

It is interesting to compare Eq. 6 to the corresponding recursive transcendental Eq. I.22 in the simple voltage recording solution. We note that the roots of Eq. 6, when all the stem segments are considered, are the singularities of Eq.

[2] The same convention is followed in Refs. 7 and 8. By contrast, in Refs. 2, 3, and 9 the indexing starts from 1, to emphasize the distinction between the slowest voltage clamp time constant and the membrane time constant $\tau_m = R_m C_m$, which is the same as τ_0 only when $g_{\text{shunt}} = 0$.

I.22. Thus the cell as a whole generates a voltage clamp eigenvalue between every pair of current clamp eigenvalues. The soma (if at the clamp point) has no effect on the perfect voltage clamp eigenvalues.

For a stem segment which has no daughters, i.e., for which $\mu_{st} = 0$, it can be seen that

$$\cos \alpha L_{st} = 0, \tag{7}$$

(compare with Eq. 28 in Ref. 2). The roots are $\alpha_n = (2n + 1)\pi/2L_{st}$, $n = 0, 1, 2, \ldots$.

Time constants

As in Paper I, for each eigenvalue α_n, there is a time constant τ_n, defined by Eq. I.24. For a single cylinder model, the time constant ratios are

$$\frac{\tau_0}{\tau_n} = \frac{4L^2 + (2n + 1)^2\pi^2}{4L^2 + \pi^2}. \tag{8}$$

This constraint can prove useful when fitting exponentials to experimentally recorded voltage clamp responses.

Continuous spatial eigenfunctions

For each eigenvalue α_n, we may define an associated eigenfunction $\psi_{jn}(X_j)$. Writing Eq. 4 as

$$y_j(X_j) \equiv D_n \psi_{jn}(X_j), \tag{9}$$

with κ_{jn} and μ_{jn} the values of κ_j and μ_j at $\alpha = \alpha_n$, we have, as in Paper I,

$$\psi_{jn}(X_j) = \kappa_{jn}[\cos \alpha_n(L_j - X_j) + \mu_{jn} \sin \alpha_n(L_j - X_j)], \tag{10}$$

with the revised iterative definition Eqs. 5 and I.28 for κ_{jn}.

Using the transcendental equation (Eq. 6), the expression in Eq. 10 can be simplified for stem segments *st*, to the form

$$\psi_{stn}(X_{st}) = \frac{\sin \alpha_n X_{st}}{\sin \alpha_n L_{st}}. \tag{11}$$

Amplitudes

By linear superposition of the solutions of the form (Eq. I.13), using Eqs. I.24 and 9, the general solution to the cell's voltage response can again be written as

$$V_r(X_r, Z_e, t) = \sum_{n=0}^{\infty} D_n \psi_{rn}(X_r) e^{-t/\tau_n}. \tag{12}$$

As explained in Paper I, the α_n values in general lead to nonorthogonal eigenfunctions. In Appendix 1, we give an outline of the derivation of the amplitude terms using complex analysis. Let $\mathcal{S}(j)$ be the *stem* segment of j. The stimulation segment is e, and the recording segment is r (neither, either, or both could be the somatic clamp point s). We find that we can write the coefficients D_n as

$$D_n \equiv E_{n_{\mathcal{S}(e)}} \psi_{en}(Z_e), \tag{13}$$

where

$$E_{n_{st}} \equiv \begin{cases} \dfrac{2}{\tau_m \sum\limits_{j \in subtree(st)} g_{\infty_j} \kappa_{jn}^2 L_j (1 + \mu_{jn}^2)} & \text{if } \left\{ \begin{array}{c} \cot \alpha_n L_{st} + \mu_{stn} = 0 \\ \text{and} \\ \mathcal{S}(e) = \mathcal{S}(r) = st \end{array} \right\} \\ 0 & \text{otherwise,} \end{cases} \tag{14}$$

i.e. the summation is only over segments in the subtree with stem *st*, from which the eigenvalue α_n was generated, and $E_{n_{st}}$ is zero if the stimulation and recording segments are not both in that subtree. This is equivalent to saying that the clamp decouples the different dendritic trees at the soma (e.g., Ref. 3). The clamp point is taken to belong to all subtrees: i.e., if the input is into the clamp point, e is set to *st*, and if recording is from the clamp point, r is set to *st*.

The amplitude terms can also be derived from Eq. I.34. Let *st* be the stem segment of the source tree of a particular α_n. Let $g_s \to \infty$, $\epsilon \to 0$, and multiply the denominator by $(\cos \alpha_n L_{st} + \mu_{st} \sin \alpha_n L_{st})^2$, which tends to zero (compare with Eq. 6). The terms including g_s, and all terms from subtrees other than the one with stem *st*, tend to zero. We are left with the expression in Eq. 14 if we redefine κ_{st} to be 1. Now multiply both ψ_{en} and ψ_{rn} in Eq. I.33 by $(\cos \alpha_n L_{st} + \mu_{st} \sin \alpha_n L_{st})$: the spatial eigenfunctions tend to zero if they are not in the source tree for that α_n. If they are in the correct source tree, they become identical to the spatial eigenfunctions defined above, with $\kappa_{st} = 1$. A separate program has been written for the perfect voltage clamp solution, although the voltage recording solution does indeed generate the same time constants, amplitudes, and waveforms when g_{shunt} is extremely large, e.g., of the order 10^5–10^9 nS (but not so large that lack of numerical precision becomes a problem).

Let the cell's voltage response take the form

$$v_r(x_r, z_e, t) \equiv V_r(X_r, Z_e, t) = \sum_{n=0}^{\infty} A_{n_{er}}^{vq} e^{-t/\tau_n}, \tag{15}$$

with superscript *vq* indicating voltage recording away from the clamp point, for a unit point charge input (q). The subsubscripts e and r are the input (excited) and recording segment as usual. Thus the amplitude terms of the transient components, by comparison with Eq. 12 and using Eq. 13, can be written as

$$A_{n_{er}}^{vq} = E_{n_{\mathcal{S}(e)}} \psi_{en}(Z_e) \psi_{rn}(X_r). \tag{16}$$

Note that, within the source tree of α_n, the amplitude term is the product of three factors: $E_{n_{\mathcal{S}(e)}}$ which is a constant over

the whole source tree (zero if excitation and recording sites are not both within that tree), $\psi_{en}(Z_e)$ which depends on the excitation site, and $\psi_{rn}(X_r)$ which depends on the recording site. As with the voltage recording solution in Paper I, interchanging stimulation and recording sites does not alter the voltage transients.

Clamp current

Let the clamp current i_{clamp} be

$$i_{\text{clamp}}(Z_e, t) = \sum_{n=0}^{\infty} A_{n_e}^{iq} e^{-t/\tau_n}, \tag{17}$$

with superscript *iq* indicating current (i) recording at the clamp point at the origin of segment *st*, for a unit point charge input (q) into segment *e*.

Then, since the clamp current must equal the axial current to prevent voltage changes at the soma,

$$i_{\text{clamp}} = -g_{\infty_{\not e(e)}} (\partial V_{\not e(e)}/\partial X_{\not e(e)})|_{X_{\not e(e)}=0}, \tag{18}$$

we have from Eqs. 11, 15, and 16:

$$A_{n_e}^{iq} = -\alpha_n g_{\infty_{\not e(e)}} E_{n_{\not e(e)}} \psi_{en}(Z_e)/\sin \alpha_n L_{\not e(e)}. \tag{19}$$

Repeated eigenvalues

In cases where both the stimulation and recording sites are at the clamp point, and for some reason of symmetry two or more different subtrees produce the same eigenvalue, the clamp currents from the individual subtrees are still independent and still add linearly.

Singularity coincidences

As in the previous paper, there is the possibility of singularity clashes whenever two different subtrees or segments within a particular dendritic tree produce singularities at the same value of α_n. The problem is dealt with in exactly the same way as in the previous paper, except that there is no parallel in the voltage clamp case to the *n*-cylinder special amplitude terms (Eqs. I.112 and I.113).

Case II: Solution for a unit voltage command impulse

Amplitudes

The details of the solution of Eqs. I.3–I.7, 1, and 3 follow closely the unit charge input case already considered. The separable solutions are still of the form of Eq. I.13 with the spatial solution of the form of Eq. 4. The boundary conditions still allow us to define the recursive transcendental equation given by Eqs. 6, I.19, and I.20, and the recursive continuity factors (Eq. I.28). Thus we have the same eigenvalues as in the unit charge impulse case, and hence the same time constants (Eq. I.24). The associated eigenfunctions are again defined by Eq. 10, with the simplification (Eq. 11) for stem segments *st*. However, the amplitudes are different. Using Laplace transforms (see Appendix 1, Case II), the coefficients D_n can be shown to be

$$D_n \equiv \alpha_n g_{\infty_{\not e(r)}} E_{n_{\not e(r)}}/\sin \alpha_n L_{\not e(r)}. \tag{20}$$

Thus, writing the transient voltage response of the cell as follows,

$$v_r(x_r, z_e, t) \equiv V_r(X_r, Z_e, t) = \sum_{n=0}^{\infty} A_{n_r}^{vv} e^{-t/\tau_n}, \tag{21}$$

where the superscript *vv* indicates voltage recording away from the clamp point for a unit voltage command impulse, the amplitudes are given by

$$A_{n_r}^{vv} = \alpha_n g_{\infty_{\not e(r)}} E_{n_{\not e(r)}} \psi_{rn}(X_r)/\sin \alpha_n L_{\not e(r)}. \tag{22}$$

Clamp current

Using the relation (Eq. 18) and the expression (Eq. 21), we have

$$i_{\text{clamp}}(t) = \sum_{n=0}^{\infty} A_n^{iv} e^{-t/\tau_n}, \tag{23}$$

where superscript *iv* indicates current recording (i) for a unit voltage command impulse, and where

$$A_n^{iv} = -(g_{\infty_{st}} \alpha_n)^2 E_{n_{st}}/\sin^2 \alpha_n L_{st}. \tag{24}$$

The coefficients $E_{n_{st}}$ are defined in Eq. 14. We remark that the clamp point is taken to be the origin of segment *st*, the stem of the source tree of α_n.

Symmetries between cases I and II

We note that the expressions (Eqs. 22 and 24) for Case II, the response to a somatic voltage command impulse, are the same as the corresponding terms for Case I, the unit charge impulse into a dendrite, with $\psi_{en}(Z_e)$ replaced by $\alpha_n g_{\infty_{\not e(r)}}/\sin \alpha_n L_{\not e(r)}$ (compare Eq. 13 with Eq. 20).

Comparing Eqs. 19 and 22 reveals that the voltage response of Case II is simply the negative of the clamp current of Case I, with the stimulating and recording positions reversed. This relationship could be usefully exploited in compartmental model simulations. Where the clamp currents in response to the same input current at a number of different sites are required, instead of simulating each case individually, the input waveform can be applied to the soma as a voltage command, and the voltage responses at all of the sites of interest can be monitored simultaneously in one run. The desired clamp currents are then simply the voltage responses inverted.

Parameter dependence (perfect clamp)

As in Paper I, the important equations determining the solution can be rearranged to show more clearly the dependencies on the "raw" electrical parameters C_m, R_m, and R_i.

As before, Eq. I.19, for the μ_j factors can be re-written as Eq. I.39. Equation 14 becomes

$$E_{n_{st}} = \begin{cases} \dfrac{2}{C_m \sum\limits_{j \in subtree(st)} a_j \kappa_{jn}^2 (1 + \mu_{jn}^2)} & \text{if } \left\{ \begin{array}{c} \cot \alpha_n L_{st} + \mu_{stn} = 0, \\ \text{and} \\ \mathscr{S}(e) = \mathscr{S}(r) = st \end{array} \right\} \\ 0 & \text{otherwise,} \end{cases} \quad (25)$$

where $a_j = \pi l_j d_j$ is the surface area of segment j. In the case of the n-cylinder model (5), this simplifies to $E_{n_{st}} = 2/c_{st}$, where c_{st} is the capacitance of the segment for which $\cos \alpha_n L_{st} = 0$. The solution is the linear sum of the component single cylinder solutions.

As in Paper I (the Parameter Dependence section), the α_n values will be independent of C_m and proportional to $R_m^{1/2}$. The dependencies of the time constants on C_m and R_m are also the same as those described in Paper I. The μ_{jn}, κ_{jn}, and $\psi_{jn}(X_j)$ terms are independent of C_m, R_m, and R_i (see below for the last of these). The $E_{n_{st}}$ terms are independent of R_m and R_i (again, see below for the latter) and are inversely proportional to C_m.

The transcendental equation (Eq. 6) for the eigenvalues α_n must continue to hold as R_i changes. This is certainly the case if the values of $\alpha_n L$ and, therefore, all the μ_{jn} and κ_{jn} terms are conserved, which requires $\alpha_n = \eta_n R_i^{-1/2}$, for a new variable $\eta = \alpha R_i^{1/2}$ (see Paper I). The $\psi_{jn}(X_j)$ terms will therefore be independent of R_i. The time constants are given by $\tau_n = \tau_m/(1 + \eta_n^2/R_i)$ and thus the faster ones (i.e. η large) are proportional to R_i. It can be seen from Eq. 25 that all the $E_{n_{st}}$ terms will therefore be independent of R_i; they are determined only by C_m and the geometry. The faster time constants are proportional to $R_i C_m$ and are independent of R_m. The slower time constants depend on all three parameters.

We note again that $g_{\infty_j} = (\pi/2)(R_m R_i)^{-1/2} d_j^{3/2}$. The synaptic input voltage response amplitude terms $A_{n_{er}}^{vq}$ in Eq. 16 will show the same dependencies as the $E_{n_{st}}$ terms. The clamp current amplitude terms $A_{n_e}^{iq}$ in Eq. 19 contain an additional factor of the form $\alpha_n g_{\infty_j}$ and so are independent of R_m and inversely proportional to R_i, as are the voltage command voltage response amplitude terms $A_{n_r}^{vv}$ in Eq. 22. The voltage command clamp current amplitude terms A_n^{iv} in Eq. 24 contain the factor $(\alpha_n g_{\infty_{st}})^2$ and so are independent of R_m and inversely proportional to R_i^2.

It should be noted that, as in Paper I, the amplitude term parameter dependencies are for the impulse responses only: upon convolving the responses with various input functions (see next section) additional factors are introduced into the amplitude expressions, further complicating the picture. However, for fast inputs the dependencies shown by the impulse responses will still apply approximately.

As before, because neither fast amplitudes nor time constants are altered by changes in R_m, the fast amplitudes of the responses to arbitrary inputs are also independent of R_m. This result deserves to be emphasized: increasing R_m experimentally, for example by using channel blockers, will have only a limited effect on the subsynaptic voltage swing and the clamp current (10), predominantly at later times when the waveform has largely decayed away (for an example, see Paper III (6), Fig. 9).

Responses to arbitrary inputs

Case I: Synaptic inputs

The results in the section Responses to Other Inputs in the previous paper may be used for the voltage clamp case. The corresponding expressions for voltage clamp are obtained by replacing the amplitude terms $A_{n_{er}}$ in Eqs. I.46, I.48, I.50 and I.52 with $A_{n_{er}}^{vq}$ or $A_{n_{er}}^{iq}$ as appropriate, to obtain the voltage transients and the clamp currents respectively, for the various example input functions.

The lumped and steady-state terms for voltages are as described in Appendices 2 and 3 of the previous paper, with $\bar{A}_s = 0$ (see also for definitions of some of the following terms). The lumped amplitude terms for clamp currents are given by the following.

$$-g_{\infty_{\mathscr{S}(e)}} \frac{dH_{er}}{dX_{\mathscr{S}(e)}} \bigg|_{X_{\mathscr{S}(e)}=0}. \quad (26)$$

Therefore, instead of $\bar{G}_r(X_r, Z_e, p)$ in the relevant expression for H_{er} (defined in Paper I, Appendix 2), substitute

$$-g_{\infty_{\mathscr{S}(e)}} q \bar{\kappa}_{\mathscr{S}(e)} \bar{B}_{\mathscr{S}(e)} = -\bar{\kappa}_e [\cosh q(L_e - Z_e) + \bar{\mu}_e \sinh q(L_e - Z_e)], \quad (27)$$

(differentiating Eq. I.68 with $c = \mathscr{S}(e)$, bearing in mind that $\bar{A}_s = 0$ in this case, since $V_{com} = 0$). As before, if $\tau_{sy} < \tau_m$, i.e. $q = iw$, use the substitutions (I.88) and Eqs. I.96–I.102, as detailed in Paper I, Appendix 2, with $A_s' = 0$. Note that in these cases the κ_{st} term is defined by Eq. I.30, with w instead of α_n and dropping subscript n. Again, for the steady-state, $q = 1$.

Case II: Voltage commands

(I) Voltage step Integrating the impulse response Eq. 21 with respect to time, the voltage response to a command step V_{step} imposed at $t = 0$ at the clamp point is

$$v_r(x_r, t) = \hat{v}_r(x_r) - \sum_{n=0}^{\infty} V_{step} \tau_n A_{n_r}^{vv} e^{-t/\tau_n}, \quad (28)$$

where

$$\hat{v}_r(x_r) = V_{step} \hat{\kappa}_r [\cosh(L_r - X_r) + \hat{\mu}_r \sinh(L_r - X_r)], \quad (29)$$

where $\hat{\kappa}_j = \bar{\kappa}_j$ with $q = 1$ (Eq. I.66) and where $\hat{\mu}_j$, the steady-state branching factor of segment j, is defined recursively by

$$\hat{\mu}_p = g_{\infty_p}^{-1} \sum_{d \in dtrs_p} g_{\infty_d} \frac{(1 + \hat{\mu}_d \coth L_d)}{(\coth L_d + \hat{\mu}_d)} \quad (30)$$

(cf. Eq. I.64 with $q = 1$). For single cylinders, Eq. 28 can be reduced to Eq. 5 in Ref. 3. Equations 29 and 30 are equivalent to Rall's branching steady-state solution (11); using V instead of $\bar{G}$, the *steady-state* differential equations are Eq. I.58, with $p = 0$ and right hand side always zero, Eq. I.59, Eq. I.60, and $V_s = V_{step}$.

Since $A_{n_r}^{vv} \propto (R_i C_m)^{-1}$, and the fast τ_n values are proportional to $R_i C_m$, the fast transient amplitudes of the step response voltage in Eq. 28 will be independent of *all* raw electrical parameters and will depend only on the morphology. The slow transient amplitudes will be independent of C_m.

Similarly, integrating Eq. 23 with respect to time, the clamp current is

$$i_{clamp}(t) = V_{step}/R_{ss} - \sum_{n=0}^{\infty} V_{step}\tau_n A_n^{iv} e^{-t/\tau_n}, \qquad (31)$$

where R_{ss} is the input resistance measured at the clamp point (the soma). This is given in Ref. 11 or by $\bar{A}_s$ in Eq. I.78, with $q = 1$ and the numerator set to 1:

$$R_{ss} = \left\{ g_s + \sum_{st \in stems} g_{\infty_{st}} \frac{(1 + \hat{\mu}_{st} \coth L_{st})}{(\coth L_{st} + \hat{\mu}_{st})} \right\}^{-1}. \qquad (32)$$

Note that the transient amplitude terms all have the same sign as V_{step}, since the A_n^{iv} terms, given by Eq. 24, are negative. In the case of a single cylinder + soma model, Eq. 31 can be simplified to

$$i_{clamp}(t) = V_{step}\left(g_s + g_\infty \tanh L + \sum_{n=0}^{\infty} \frac{2\alpha_n^2 g_\infty}{(1 + \alpha_n^2)L} e^{-t/\tau_n} \right), \qquad (33)$$

where the α_n values are odd integer multiples of $\pi/2L$. This solution is consistent with Eq. 8 in Ref. 3 and Eq. 12 in Ref. 9. For a single cylinder model, the amplitude ratios are

$$\frac{A_n}{A_0} = \frac{(2n + 1)^2(4L^2 + \pi^2)}{4L^2 + (2n + 1)^2\pi^2}. \qquad (34)$$

This additional constraint may be useful when performing exponential fitting to experimentally recorded clamp currents.

Since $A_n^{iv} \propto (R_i^2 C_m)^{-1}$, the fast current amplitudes, following a voltage step, are inversely proportional to R_i, and are independent of all the other raw electrical parameters (Eq. 31). All the amplitudes are independent of C_m. In direct fits to the step voltage charging current, therefore, the fast amplitudes will constrain R_i, the fast τ_n values will then constrain C_m, and the slow amplitudes and time constants will constrain R_m.

(ii) Arbitrary voltage commands The impulse response (Eq. 21) can be convolved numerically with any arbitrary voltage command waveform (e.g., an action potential waveform measured experimentally), to obtain the model's response to such a stimulus. The impulse response can also be convolved analytically with all the input functions given in the previous paper, using the same working, to obtain analogous responses (including the lumped terms), replacing $A_{n_{er}}$ with $A_{n_r}^{vv}$ for the voltage responses away from the clamp point, and with A_n^{iv} for the clamp currents (as with the two examples above). Q, the total input charge, in the other cases is replaced by the time integral of the command voltage (the total "volts-seconds" injected). In the lumped terms for the voltages, G_j is redefined to be the response to a voltage impulse and $\bar{G}_j$ is given by Eq. I.67, with $\bar{A}_s = 1$. When q is imaginary, as is discussed in Appendix 2 of the previous paper, Eq. I.94 should be used. In the lumped terms for the clamp currents, apply Eq. 26 to Eq. I.67 and sum over all the stem segments, then include the appropriate terms for the soma conductance and capacitance in the Laplace domain (left-hand side of Eq. I.61), to replace $\bar{G}_r(X_r, Z_e, p)$ in H_{ststst} with

$$g_s[1 + \epsilon(q^2 - 1)] + q \sum_{st \in stems} g_{\infty_{st}} \bar{\kappa}_{st}[\sinh qL_{st} + \bar{\mu}_{st} \cosh qL_{st}]. \qquad (35)$$

This complex input admittance is identical to the denominator of Eq. I.78. When q is imaginary, replace this with the denominator of Eq. I.95. Notice the steady-state responses above are the special case of these lumped terms with $q = 1$.

IMPERFECT VOLTAGE CLAMP

Comparison to voltage recording with a shunt

It is common in experiments for there to be a series resistance R_{ser} (conductance g_{ser}) between the clamp amplifier and the recording site in the cell. The voltage at the recording site does not perfectly track the voltage command, and the clamp current is distorted. Voltage responses recorded in the presence of a shunt can be thought of as being imperfectly voltage-clamped to the reversal potential of the shunt. The voltage deflection at the recording site is identical to the voltage escape there when clamping to the same reversal potential via a series conductance equal to the shunt conductance.

Any response can be separated into a transient and a steady-state component. For a step or impulse command at $t = 0$, the transient component of the voltage at the amplifier end of the series resistance is always zero at times $t > 0$. The conventions adopted here are that earth, resting membrane potential, and shunt reversal potential are all taken to be zero. In other words, from the point of view of the transient part of the response, the series conductance is formally equivalent to a shunt to earth. We remark that for the steady-state component, the reversal potential of this extra shunt is the steady-state command voltage.

Mathematically, the model equations now change slightly. A series conductance g_{ser} between the clamp amplifier and soma is equivalent to introducing an *extra* shunt conductance in parallel to the total soma conductance (which already includes any electrode-induced shunt). Thus we redefine

the somatic conductance to include the series conductance as follows,

$$g_s^* = g_s + g_{ser} = g_{sm} + g_{shunt} + g_{ser}, \tag{36}$$

and the somatic shunt parameter now becomes

$$\epsilon^* = c_s/(g_s^*\tau_m). \tag{37}$$

The mathematical equations describing this model are now given by Eqs. I.3–I.7, together with the new somatic boundary condition,

$$g_{ser}V_{com}(t) = g_s^*\left(V_s + \epsilon^*\tau_m\frac{\partial V_s}{\partial t}\right) - \sum_{st\in stems} g_{\infty_{st}}\frac{\partial V_{st}(X_{st})}{\partial X_{st}}\bigg|_{X_{st}=0}, \tag{38}$$

(compare with Eq. I.8). The transcendental equation for the eigenvalues α_n is the same as Eq. I.22 with ϵ^* and g_s^* substituted for ϵ and g_s, respectively. As before, the time constants are given by Eq. I.24.

As in the perfect voltage clamp case, we consider the following two cases, which can be added linearly:

Case I: Synaptic inputs

In this case, $V_{com}(t) = 0$ and the series conductance is also equivalent to a shunt to earth for the steady state part of the solution. This system is identical to simple voltage recording with an *extra* shunt conductance in parallel to the total "soma" conductance (already including any electrode-induced shunt). The responses to synaptic inputs in this case, are obtained from the solutions in Paper I simply by replacing g_s and ϵ with g_s^* and ϵ^*, respectively.

The clamp current is then given by

$$i_{clamp} = -g_{ser}V_s, \tag{39}$$

where V_s is the voltage at the cell end of the series resistance (soma). It follows that

$$A_{n_e}^{iq} = -g_{ser}E_n\psi_e(Z_e), \tag{40}$$

where E_n is given in Eq. I.34, using g_s^* and ϵ^*. The κ_{st} of all the stem segments *st* are as in Eq. I.30. In other words, when "synaptic" currents are recorded with a steady zero command potential, the series conductance is added to the somatic shunt and *the clamp current is an attenuated, upside-down version of the postsynaptic potential recorded at the soma.*

Case II: Voltage commands

Voltage command impulse response

It can be shown (see Appendix 2) that in response to a unit voltage impulse command $V_{com}(t) = \delta(t)$, the cell's response under imperfect clamp is given by Eq. 21, the α_n values in Eq. I.24 being the roots of Eq. I.22 with g_s^* and ϵ^* replacing g_s and ϵ. We obtain $D_n = g_{ser}E_n$, and amplitude terms

$$A_{n_r}^{vv} = g_{ser}E_n\psi_r(X_r), \tag{41}$$

again using the definitions in Paper I with g_s^* and ϵ^*. Note that, as with perfect clamp, the reciprocity relation $A_{n_e}^{iq} = -A_{n_r}^{vv}$ holds, i.e., the dendritic voltage response to a somatic voltage command is the negative of the somatic clamp current in response to a current input of the same time-course and magnitude at the same dendritic site (with appropriate units).

From Eq. 39, the clamp current when $t > 0$ is given by Eq. 23 with

$$A_n^{iv} = -g_{ser}^2E_n. \tag{42}$$

Steps and other voltage commands

Since D_n values for the response to a unit voltage impulse are given by $g_{ser}E_n$, and in Paper I the D_n values in response to a unit current impulse (point charge) were given by $E_n\psi_{en}(Z_e)$, the voltage response to any other voltage command function is simply g_{ser} times the solution for the equivalent current injection function in Paper I, with $\psi_{en}(Z_e) = 1$ (since the input is into the soma) and $V_{com}(t)$ replacing the input current $i(t)$.

For example, the voltage response to a *voltage command step* at $t = 0$ of magnitude V_{step} can be obtained in this way from Eq. I.46, substituting V_{step} for i_{in}. Alternatively, Eq. 21 can be integrated with respect to time. The solution is

$$v_r(x_r, t) = \hat{v}_r(x_r) - \sum_{n=0}^{\infty} V_{step}g_{ser}\tau_nE_n\psi_r(X_r)e^{-t/\tau_n}, \tag{43}$$

The steady-state term is given by

$$\hat{v}_r(x_r) = \hat{v}_s\hat{\kappa}_r[\cosh(L_r - X_r) + \hat{\mu}_r\sinh(L_r - X_r)]. \tag{44}$$

This can be obtained from Eq. I.110 or by noting that the series resistance and cell input resistance act as a voltage divider, so the steady state voltage at the soma $\hat{v}_s$ is given by

$$\hat{v}_s = V_{step}R_{ss}/(R_{ser} + R_{ss}) = V_{step}g_{ser}R_{ss}^*, \tag{45}$$

where R_{ss}^* is the combined input resistance of the cell in parallel with g_{ser}, given by substituting g_s^* for g_s in Eq. 32.

In all cases the clamp currents are given by

$$i_{clamp}(t) = g_{ser}[V_{com}(t) - v_s(t)], \tag{46}$$

where $v_s(t)$ is the soma voltage. In particular, the clamp current for a step command is

$$i_{clamp}(t) = g_{ser}(V_{step} - \hat{v}_s) + \sum_{n=0}^{\infty} V_{step}g_{ser}^2\tau_nE_ne^{-t/\tau_n}. \tag{47}$$

The steady-state current can be simplified to $V_{step}/(R_{ser} +$

R_{ss}), which can also be obtained more directly by noting that R_{ser} and the cell's input resistance R_{ss} are in series. The fast current amplitudes are proportional to R_i, independent of R_m and C_m, and are proportional to g_{ser}^2. The slow amplitudes are independent of C_m. Because E_n is never negative (see Paper I, Parameter Dependence section), all the amplitude terms have the same sign as V_{step}, an important constraint when fitting multiple exponentials to model or experimental clamp currents.

For a single cylinder + soma model, Eq. 47 simplifies to

$$i_{clamp}(t) = \frac{V_{step}}{R_{ser} + (g_s + g_\infty \tanh L)^{-1}} + \sum_{n=0}^{\infty} \frac{2V_{step} g_{ser}^2 e^{-t/\tau_n}}{(1 + \alpha_n^2)[g_s^*(2\epsilon^* + \theta_n^*) + g_\infty L \sec^2 \alpha_n L]}, \quad (48)$$

where

$$\theta_n^* \equiv [1 - \epsilon^*(1 + \alpha_n^2)]/\alpha_n^2. \quad (49)$$

This is the exact solution corresponding to the approximate form derived by Jackson (9).

Limiting behavior as $g_{ser} \to \infty$

No-shunt voltage recording and perfect voltage clamp are the two extremes of imperfect clamp. As $g_{ser} \to 0$, the solution tends to the no-shunt voltage recording case (see Paper I). As $g_{ser} \to \infty$, the transcendental equation (Eq. I.22), with g_s^* and ϵ^*, tends to the perfect voltage clamp transcendental equation (Eq. 6), since for Eq. I.22 to balance in this limit, we must necessarily have one of the denominator terms on its right hand side as zero.

As mentioned above, careful consideration of the limiting behavior of the κ and other terms in Eqs. I.33 and I.34 as $g_s^* \to \infty$ and $\epsilon^* \to 0$, shows that the amplitude expressions tend to those of the voltage clamp case, including the property that they are zero if the recording and stimulating segments are not in the same dendritic tree.

Parameter dependence of imperfect clamp impulse response

General

The dependencies of the imperfect voltage clamp solution time constants and voltage response amplitudes in Case I (synaptic inputs) are necessarily the same as those of the solution in Paper I for voltage recording with a somatic shunt, given their mathematical equivalence. The Case I clamp current fast amplitude terms are proportional to $g_{ser} C_m^{-1}$ as are those of the Case II (voltage commands) voltage responses. Case II clamp current fast amplitudes are proportional to $g_{ser}^2 C_m^{-1}$. All slow amplitudes are proportional to C_m^{-1} and change with R_i, g_{ser}, and g_{shunt}. As in Paper I, all amplitudes are independent of R_m. As before, the α_n values will be proportional to $R_m^{1/2}$, and all the faster time constants will be independent of R_m.

Large soma, thin dendrites case

Following the discussion of the transcendental equation in Ref. 9, we consider the roots of the transcendental equation (Eq. I.41) when R_{ser} is very small, i.e., when g_{ser} is very large. For the rest of the discussion on parameter dependence we shall assume g_{ser}, the conductance between cell and amplifier, is synonymous with g_{shunt}, and that there is no additional shunt to true earth.

(i) Small roots: when $g_{ser} \gg \alpha^2/R_{sm}$, i.e., $\alpha^2 \ll R = R_{sm}/R_{ser}$, the roots occur near the locations of the positive singularities on the right-hand side (compare with Eq. 6). Thus, as noted previously (9), the smaller α_n values and the slower time constants and amplitudes are approximately the same as with perfect clamp.

(ii) Intermediate root(s): when $\alpha^2 \approx R$, the roots occur near the zeroes of the right-most term in Eq. I.41, and $\tau_n \approx \tau_m/R = R_{ser} c_s$.

(iii) Large roots: when $\alpha^2 \gg R$ each α_n occurs near a negative singularity on the right-hand side of Eq. I.41, i.e., near α_{n-1} of the perfect voltage clamp case.

As noted for the single cylinder case in Ref. 9, these approximations are best when the sum of the stem segment ρ_∞ values ($= g_\infty/g_{sm}$ values, here) is small (i.e., when the dendrites are thin compared with the soma diameter and when $\sqrt{R_m/R_i}$ is small, see Paper III, Eq. 2). Anatomical and electrophysiological data suggest, however, that this is unlikely for many pyramidal neurones (see Paper III (6), Example 1), and the parameter estimation methods outlined in Ref. 9 may break down in practice for such cells. In such cases there is a large number of intermediate roots which are not close to either the singularities or the zeroes of the right-most term in Eq. I.41.

In examples where the approximations hold, all but the intermediate α_n values are roughly proportional to $R_i^{-1/2}$ and the faster time constants are approximately proportional to $R_i C_m$. All but the intermediate amplitude terms are independent of R_i (as in the perfect clamp case). In cases where the approximations break down, the amplitude terms display no simple dependence on R_i.

Time constants and R_{ser}

As in Paper I, Example 2, the "effective" time constants τ_{eff} of clamp current waveforms are very sensitive to the fit interval chosen, and may be very different from the true τ_0 of the model, being either slower or faster. τ_{eff} can be defined to be the time constant of the optimal single exponential fit over a *standard* interval relative to the peak time t_{peak}, e.g., t_{peak} + 0.7 to t_{peak} + 20 ms (12). Depending on the signal-to-noise ratio, a more universal measure might be τ_{7525}, the effective time constant over an interval from t_{75} to t_{25}, where $t_{a\%}$ is the time following the peak at which the response has

fallen to $ab\%$ of its peak value. Because $0.25/0.75 \approx 1/e$, τ_{7525} should be given, approximately, by $t_{7525} \equiv t_{25} - t_{75}$,[3] providing the decay is roughly single exponential.

Compartmental model simulations of realistic mossy fiber inputs into CA3 pyramidal cells revealed that τ_{eff}, using the convention in Ref. 12, increased from its perfect clamp value approximately linearly with R_{ser}, the series resistance, for R_{ser} less than 20 MΩ (12, 13). Similar effects are demonstrated in Paper III (6) for a single cylinder + soma model, and the CA1 pyramidal cell. To explore the factors underlying this interesting relationship, we derive the dependence of τ_0 and subsequent time constants on R_{shunt} (or R_{ser}), when R_{shunt} is small. For illustrative purposes, we consider the one-cylinder case. The transcendental equation (Eq. I.41) for the one-cylinder case, may be written as

$$g_\infty \alpha \tan(\alpha L) = \left(\frac{1}{R_{ser}} - g_{sm}\alpha^2\right) \tag{50}$$

where g_{sm} is the soma membrane conductance. In the limit $R_{ser} \to 0$, the first root $\alpha_0 \to \pi/2L$, and thus for R_{ser} small, we may write

$$\alpha_0 = \frac{\pi}{2L} - \delta \quad \text{with} \quad 0 < \delta \ll \frac{\pi}{2L}. \tag{51}$$

Substituting this expression for α_0 into the transcendental equation (Eq. 50), noting that $\tan((\pi/2) - \theta) = \cot\theta$ and rearranging, gives

$$g_\infty\left(\frac{\pi}{2L} - \delta\right) = \left[\frac{1}{R_{ser}} - g_{sm}\left(\frac{\pi}{2L} - \delta\right)^2\right]\tan(\delta L). \tag{52}$$

Expanding for small δ, we obtain

$$g_\infty \frac{\pi}{2L} = \left(g_\infty + \frac{L}{R_{ser}} - \frac{g_{sm}\pi^2}{4L}\right)\delta + O(\delta^2), \tag{52a}$$

where $O(\delta^2)$ means terms of the order of δ^2. This gives the approximation,

$$\delta \approx \frac{g_\infty \pi R_{ser}}{2L^2}\left[1 + R_{ser}\left(\frac{g_\infty}{L} - \frac{g_{sm}\pi^2}{4L^2}\right)\right]^{-1}, \tag{53}$$

which, for R_{ser} small, may be further expanded to give

$$\delta \approx \frac{g_\infty \pi}{2L^2} R_{ser}. \tag{54}$$

Now τ_0 is given by

$$\tau_0 = \frac{\tau_m}{1 + \alpha_0^2}, \tag{55}$$

which, on using Eq. 51 and expanding again for small δ, gives

$$\tau_0 = \frac{\tau_m}{1 + \dfrac{\pi^2}{4L^2}} + \frac{\tau_m \pi}{L\left(1 + \dfrac{\pi^2}{4L^2}\right)^2}\delta + O(\delta^2). \tag{56}$$

Thus, substituting Eq. 54 into Eq. 56 gives the linear approximation

$$\tau_0 \approx \frac{\tau_m}{1 + \dfrac{\pi^2}{4L^2}} + \frac{\tau_m g_\infty \pi^2}{2L^3\left(1 + \dfrac{\pi^2}{4L^2}\right)^2} R_{ser}. \tag{57}$$

To make explicit the dependence on the "raw" morphological and electrical parameters (see Paper I), this can be written

$$\tau_0 \approx \frac{16R_i l^2 R_m C_m}{16R_i l^2 + \pi^2 R_m d} + \frac{8\pi^3 l d^3 C_m R_m^2}{(16R_i l^2 + \pi^2 R_m d)^2} R_{ser}$$
$$= \tau_0^{vc} + \beta_0 R_{ser}, \tag{58}$$

where the intercept τ_0^{vc} is the slowest time constant with perfect voltage clamp, and β_0 is the slope. An example is shown in Paper III, Fig. 4 *A*.

In principle, this method may be applied to subsequent roots, and similar approximations may be obtained for the other time constants, writing τ_n instead of τ_0 and $(2n + 1)\pi$ for π in the above equations in this section (except the π^3 in the numerator of the slope term in Eq. 58, becomes $(2n + 1)^2\pi^3$), for $n = 0, 1, 2, \ldots$. As n increases, the approximations become unsatisfactory at progressively lower values of R_{ser} (see Paper III, Example 1). As noted in Paper I (Parameter Dependence section), the fastest waveform components of the voltage response are independent of R_{shunt} (i.e., R_{ser}), once it is (appreciably) greater than zero.

We remark that this method can be extended to the n-cylinder transcendental equation. In the limit $R_{ser} \to 0$, the first eigenvalue $\alpha_0 \to (\pi/2L_{max})$, where L_{max} is the largest electrotonic length of the n cylinders. The left-hand side of Eq. 50 is now the sum of n terms (see Eq. I.23). However, at the first root, the term from the longest cylinder completely dominates the others, so that the above results now apply, with L in Eq. 57 replaced with L_{max}. In Eq. 58, use the corresponding l and d.

In the fully branched case, in principle this method will still apply. However, an analytical expression for the first root α_0 when $R_{ser} = 0$ (perfect clamp) is difficult to obtain and depends on the geometry involved. Approximately linear dependence of the slowest time constants on R_{ser} has been observed empirically for complex models (e.g., the hippocampal pyramidal cell introduced in Paper I). When the "real" time constants τ_n become closely spaced, however, they have very little "room to maneuver" and change only slightly with R_{ser}. (As concluded above, the roots of the perfect voltage clamp transcendental equation are the singularities of the zero shunt voltage recording transcendental equation. τ_n is always constrained to lie between its zero shunt and perfect clamp values, a range which is always less than the interval

[3] A better approximation would be the effective time constant between t_{73} and t_{27}, $\tau_{7327} \approx t_{7327} \equiv t_{27} - t_{73}$).

between neighboring time constants.) The effective time constant versus R_{ser} plots (e.g., Paper III, Fig. 10 *D*) actually cross many individual τ_n vs. R_{ser} lines (not shown), most of which are virtually horizontal apart from an initial slight increase. The growth in τ_{eff} with R_{ser} is therefore caused both by increases in the slower τ_n values *and* by shifts in the relative weightings of the amplitudes toward slower components.

Influence of electrical parameters on effect of R_{ser}

Inspection of Eq. 58 shows that the time constants are proportional to C_m, as already determined from the full solution (see Paper I, Parameter Dependence section). In addition, raising R_m or R_i will increase the intercept term (the time constant with perfect clamp) in Eq. 58. Raising R_m or lowering R_i will also increase the slope, worsening the effects of series resistance (see Refs. 12 or 13, for an example of the latter effect). This result seems counterintuitive, since both of these maneuvers would be expected naively to improve voltage clamp by shortening electrotonic lengths. When R_i is lowered, there will be a trade-off between a decreased intercept and an increased slope.

Intuitively, the time constant with which the imperfect clamp filters the recorded waveforms will be $\tau_{clamp} \approx R_{ser}C_{eff}$ where C_{eff} is the "effective capacitance" of the cell. When R_i is decreased, there is less axial resistance "protecting" distal parts of the dendritic membrane from the clamp amplifier, and so C_{eff} and hence τ_{clamp} increase and the waveforms are more strongly smoothed. Raising R_m will have a similar effect, by improving charge transfer along the dendritic cables.

Influence of morphological parameters on effect of R_{ser}

The argument at the end of the previous section suggests that, for a given series resistance and input current, cells with a big effective capacitance will generate waveforms that are much more smoothed than those from cells with a small C_{eff}. The corollary of this is that much higher series resistances are compatible with recording fast events from "small" cells (e.g., cerebellar granule cells (14)) than from "big" cells (e.g., CA3 pyramids (12)). This is discussed further in Ref. 13 (Chapter 6).

Exactly what constitutes "big" or "small" depends on the extent to which the membrane capacitance is distributed down dendritic cables. More specifically, inspection of Eq. 58 reveals that, for a single cylinder + soma, increasing the length l or decreasing the diameter d will increase the intercept τ_0^{vc}. (Both maneuvers increase the electrotonic length of the cell.) Increasing d will always increase the slope term in Eq. 58. (Intuitively, more membrane capacitance becomes accessible to R_{ser}, both because of the increased area, and because of the decreased axial resistance.)

The effects of an increase in l on the slope are more complex. If $\pi^2 R_m d \ll 16 R_i l^2$, then the slope decreases. (Intuitively: $L \gg \pi/2$ so the electrotonic length is so large that the cell dominates the clamp in the process of charge redistribution; making it even longer further weakens the influence of the clamp, and hence the effect of R_{ser}.) If $\pi^2 R_m d \gg 16 R_i l^2$, then the slope increases. (Intuitively: $L \ll \pi/2$ so the cell is very compact electrically and adding length means adding effective capacitance.)

APPLICATIONS

All the waveforms illustrated below have been checked against transients generated by equivalent compartmental models (15) and agree extremely closely.

Example 1: CA1 pyramid cartoon: α_n, τ_n, and $E_{n_{st}}$ values

The cartoon representation of the CA1 pyramidal neurone introduced in Paper I, Fig. 4, with the same electrical parameters ($C_m = 0.7\ \mu Fcm^{-2}$, $R_m = 100{,}000\ \Omega cm^2$, $R_i = 200\ \Omega cm$, $g_{shunt} = 15$ nS), is used here for demonstration purposes. (See Paper III for additional results using this cell.)

The first ten α_n, τ_n, and $E_{n_{st}}$ values (the latter $\times 10^{-12}$) are listed in Table 2. For comparison, the α_n and τ_n values from the voltage recording case are also included (some of these numbers also appear in Paper I, Table 3).

(i) It can be seen that the perfect voltage clamp eigenvalues and time constants alternate with the voltage-recording ones, the latter model generating the slowest time constant τ_0. Without the shunt, τ_0 would be even slower, being equal to τ_m (70 ms). The shunt of course makes no difference to the perfect voltage clamp solution.

TABLE 2 CA1 pyramid cartoon: Eigenvalues and τ_n and $E_{n_{st}}$ values

n	α_n (V.R.)§	α_n (V.C.)	τ_n (V.R.)	τ_n (V.C.)	st*	E_{n_1}‡ (basal)	E_{n_5}‡ (apical)
			ms	ms		mV	mV
0	1.36		24.66				
0		2.28		11.28	5	0.000	0.110
1	2.57		9.21				
1		2.82		7.80	5	0.000	0.107
2	3.18		6.30				
2		3.75		4.65	5	0.000	0.124
3	3.83		4.47				
3		4.32		3.56	5	0.000	0.095
4	4.33		3.55				
4		4.36		3.49	1	1.438	0.000
5	4.72		3.00				
5		4.73		3.00	5	0.000	0.033
6	5.07		2.62				
6		5.08		2.61	5	0.000	0.039
7	6.19		1.78				
7		6.21		1.77	5	0.000	0.027
8	6.39		1.67				
8		6.49		1.62	5	0.000	0.233
9	6.90		1.44				
9		6.97		1.41	5	0.000	0.212

* Stem of source tree of α_n.

‡ $\times 10^{-12}$.

§ V.R., voltage recording (with a shunt); V.C., voltage clamp (perfect). Note: the basal stem is segment 1, the apical stem is segment 5.

(ii) The basal tree (stem = segment 1) contributes only one voltage clamp component out of the first ten, with a time constant of 3.49 ms and an $E_n \times 10^{-12}$ of 1.438 mV in the basal tree (and, of course, zero in the apical tree). All the other components listed originate from the apical tree, and have zero amplitude in the basal tree. The greater number of apical components reflects the greater relative electrotonic length and complexity of the apical tree, compared with the unbranched and relatively compact basal tree.

Example 2: Two cylinder + soma model

The simplified representation of a layer III cortical pyramidal neurone from Paper I is used again here to illustrate some other important features of the voltage clamp solutions. The parameters are as in Table I.4, with the exception of g_{shunt}, which is zero unless otherwise specified. (See Paper III for further applications of the solutions using a single cylinder + soma model based on the "basal" half of this model.)

Case I: Synaptic inputs, clamp to zero

Decoupling of dendritic trees. Decoupling of different dendritic trees at the clamp point is discussed previously (3). As described above, each component of the voltage clamp solution only exists in the source dendritic tree for its particular eigenvalue, when both input and recording site are in the same tree (or at the soma). Elsewhere in the cell it is zero. When "synaptic" clamp currents are recorded with the soma clamped to zero, the soma and the noninput trees are irrelevant to the final waveform. In Fig. 1, 1 pC point charges are injected into the two dendritic sites used in the previous paper. If the soma and noninput tree are detached from the model, and the simulation is repeated, exactly the same waveforms are obtained with perfect clamp. With imperfect clamp, however, this is not the case, and the waveforms from the "detached" models become progressively less like those from the intact model as the series resistance increases (not shown).

Filtering effects of dendritic cables. It can be seen in Fig. 1 that, with perfect clamp, the clamp current resulting from an "apical" input (*B*) 1000 μm (0.707 space constants) away from the soma is much smoother and slower than that from a basal input (*A*) only 500 μm (0.224 space constants) from the soma. In addition, the peak current of the apical input is approximately a factor of ten smaller than that of the basal input. These cable filtering effects are explored further in Paper III.

Filtering effects of series resistance. Also shown in Fig. 1 are the effects of various series resistances upon the apical and the basal synaptic clamp currents recorded under imperfect voltage clamp. It can be seen that series resistances above 10 MΩ lead to significant attenuation and smoothing of the recorded synaptic currents in this model. The effects of the series resistance and the dendritic cables compound one another (see also Ref. 12, Ref. 13, Chapter 6, and Paper III).

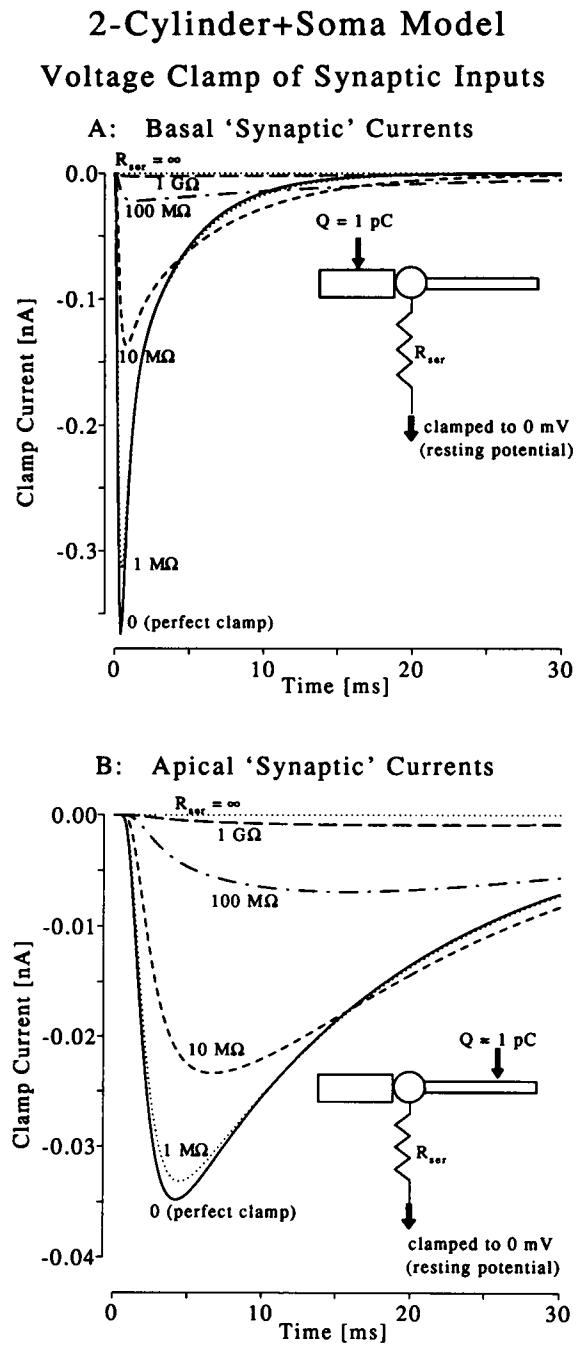

FIGURE 1 Case I: "synaptic" clamp currents under voltage clamp from the double cylinder + soma model (based on the layer III visual cortical pyramid in Paper I). Table I.4 lists the model parameters, except g_{shunt} = 0 here. The command potential is zero and 1 pC point charges are injected into the same input sites used in Paper I. Basal (*A*) and apical (*B*) synaptic currents are recorded from the soma via various series resistances R_{ser} (indicated). Different current axis scales are used in the two panels. We note that removing the noninput cylinder and the soma makes no difference to the waveforms under perfect clamp (*solid lines*), although this is not true when $R_{ser} > 0$ (not shown). The apical current is more smoothed and attenuated than the basal, and the attenuation and smoothing become worse as R_{ser} is increased. The filtering effects of the dendritic cables and series resistance therefore compound one another.

As discussed above (in the Parameter Dependence of Imperfect Clamp Impulse Response section), the value of R_{ser} that begins to cause "unacceptable" distortions of the clamp current depends very much on the morphological and electrical parameters of the cell being recorded from. It is obvious from Fig. 1 that the synaptic location is also important. Also crucial are the kinetics of the synaptic input: currents slower than the impulses used here will be less prone to smoothing by cables and series resistance. These considerations are explored in more detail in Paper III.

Effects of somatic shunt. In Fig. 2, the effects of adding a somatic shunt are illustrated for the two input locations, for a series resistance of 10 MΩ. Increasing the shunt has the effect of increasing the total conductance to zero, improving the speed of the responses at late times (the slower components are more affected than the faster ones). The responses are also smaller, since not all of the current flowing to zero is flowing via the series conductance into the hypothetical amplifier. The early parts of the responses are hardly affected by increasing g_{shunt}, and the peak currents are only slightly reduced. The peak apical clamp current occurs later than that of the basal input, and suffers a greater fractional reduction. For example, with no shunt, the peak apical current was 0.023 nA, and the peak basal current was 0.137 nA. The apparent time constants τ_{eff} obtained by "peeling" (regression interval, 10–15 ms) were 26.73 and 6.44 ms, respectively, compared with 15.66 and 3.75 ms for the perfect clamp case. When a 50-nS shunt was introduced, the peak currents were decreased to 75% (apical) and 84% (basal) of their no-shunt values. The τ_{eff} values were reduced to 21.95 and 5.57 ms, respectively.

When measuring apparent decay time constants of synaptic currents, sharp electrode recording may be superior to whole-cell recording, for a given R_{ser}: peak currents will be slightly attenuated, but the time constants will be closer to those under perfect clamp.

Case II: Voltage command step

Summation of clamp currents to different trees. In Fig. 3 the clamp current is shown when the cell is given a 1 mV command step. The cell is then broken up into its components (which are connected in parallel in the intact model): the basal tree (*b*), the apical tree (*a*), and the soma (*s*). The currents required to impose the same voltage step at the proximal end of each part are plotted. In the case of perfect clamp (Fig. 3 *A*), the sum of these three currents ($a+b+s$) is identical to the current waveform for the intact cell (*solid line*).

Effects of series resistance. The summing relationship between currents into different parts of the cell breaks down as soon as there is a series resistance: the whole-cell current falls progressively below ($a+b+s$) as R_{ser} is increased. Fig. 3 *B* shows the waveforms when R_{ser} = 10 MΩ. This *non-summing* interaction between the different parts of the cell under imperfect clamp implies that, in general, it is not possible to compensate the effects of the soma capacitance by simple subtractive techniques (cf. Ref. 16). Of course, there may be circumstances (e.g. very low R_{ser}, big soma and thin dendrites) where the interaction is approximately a summing one (Ref. 9; see Paper III, Example 1 for further discussion).

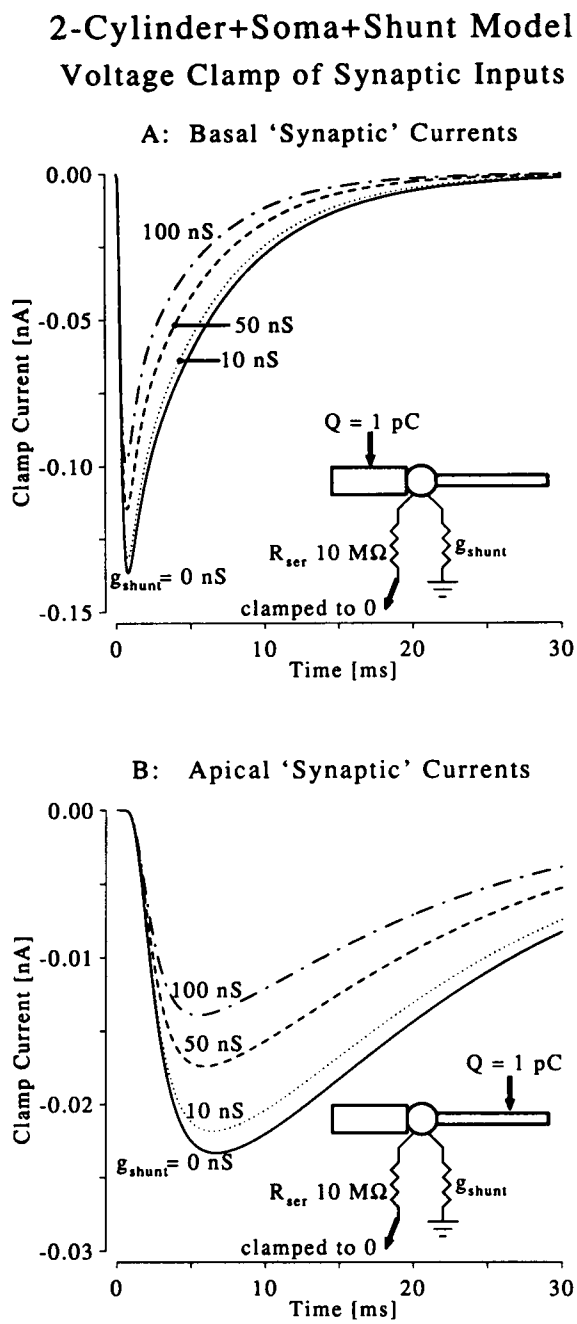

FIGURE 2 Case I: the effects of somatic shunts on synaptic clamp currents. The same model as in Fig. 1, with R_{ser} = 10 MΩ and various additional somatic shunts (indicated). The shunts mainly affect later parts of the responses, although the peaks are decreased too.

Note also that the currents in Fig. 3 *B* are slowed and have smaller early components than those recorded under perfect clamp. This phenomenon is explored further in Paper III (Example 1). The initial currents of the intact and the part models are given by V_{step}/R_{ser} = 1 mV/10 MΩ = 0.1 nA.

Fig. 4 *A* shows the actual somatic voltage in response to the command step, for different series resistances. As R_{ser} increases, the response takes longer to reach steady-state, and

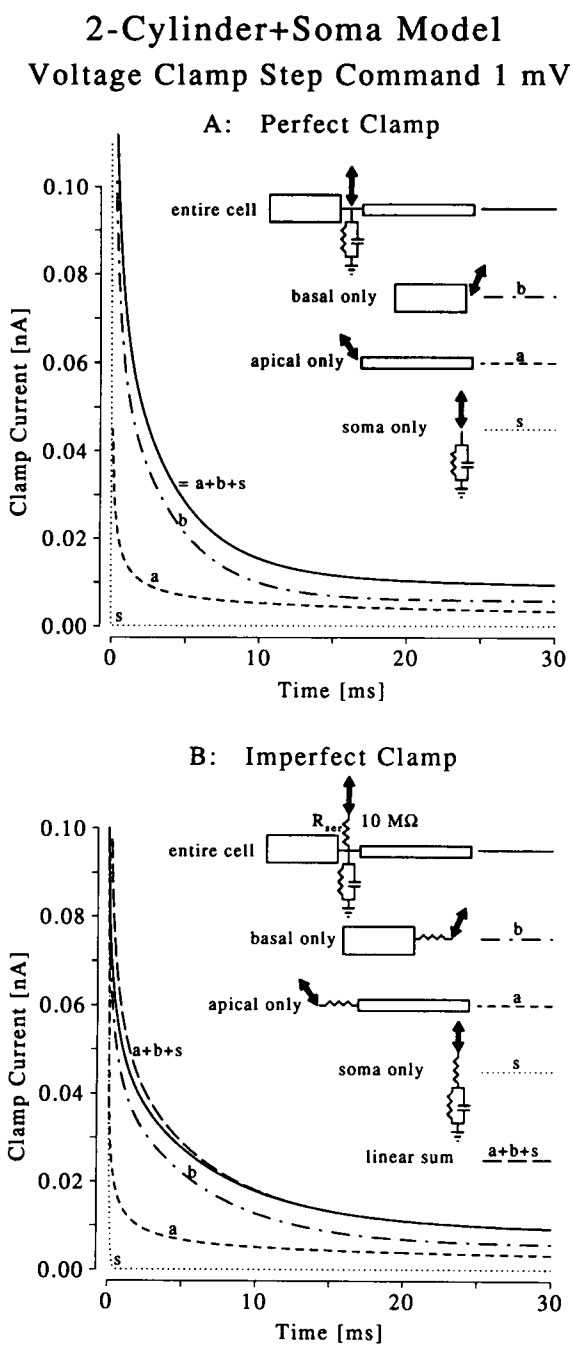

FIGURE 3 Case II: clamp currents required to impose a 1-mV voltage command step on the two-cylinder + soma model. (*A*) Perfect clamp: cell components uncoupled at clamp point. Dotted line, current into isolated soma (s); dashed line, current into isolated apical cylinder (*a*); dot-dashed line, current into isolated basal cylinder (*b*). The linear sum of the clamp currents into the three components ($a+b+s$) is the same as the clamp current for the whole cell (*solid line*). (*B*) Imperfect clamp (R_{ser} = 10 MΩ). The summing relationship breaks down as the cell components become electrically coupled. At times less than about 10 ms, the current into the whole cell (*solid line*) falls below the sum of the currents into the isolated components via the same R_{ser} (*long dashed line*, $a+b+s$).

the steady-state voltage falls increasingly below the command level. The response appears clearly inadequate with R_{ser} = 10 MΩ, taking 33 ms to approach to within 1% of the steady state of 0.92 mV.

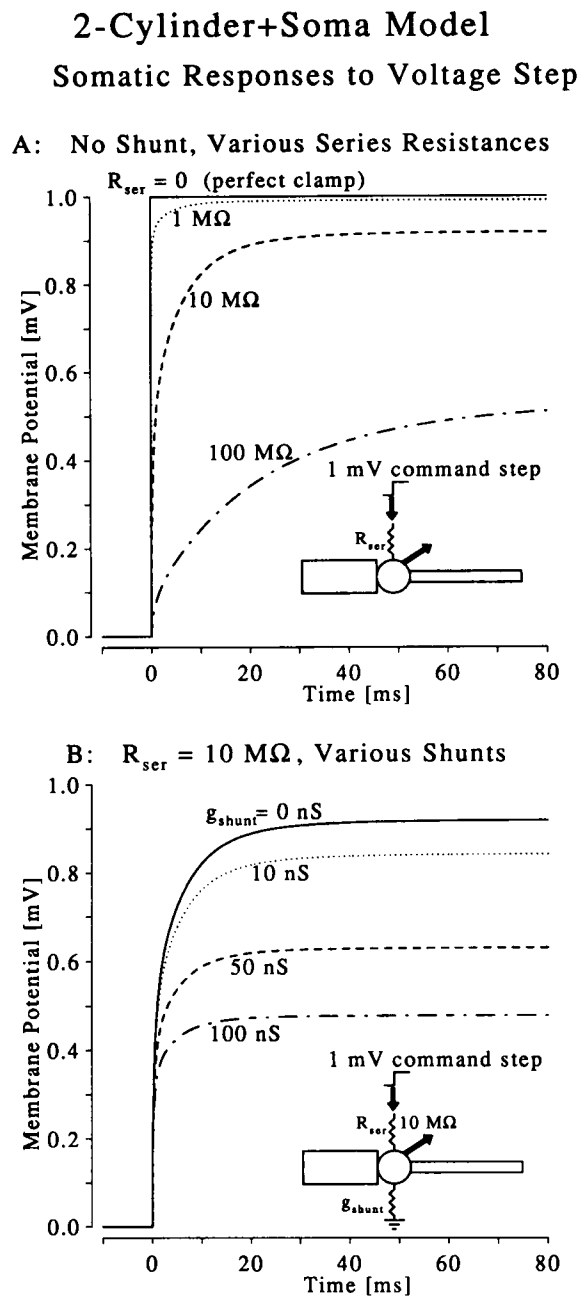

FIGURE 4 Case II: somatic voltage responses to a 1-mV step command. (*A*) Effects of various series resistances (indicated). Notice how slow and attenuated the actual response is for $R_{ser} \geq 10$ MΩ, compared with the desired step (*solid line*). (*B*) Effects of various additional somatic shunts (indicated), for R_{ser} = 10 MΩ model. Notice how the responses "square off" but reach a lower steady-state as the shunt is increased.

Effects of somatic shunt. Fig. 4 *B* shows the somatic voltage of the R_{ser} = 10 MΩ model as additional somatic shunts of various sizes are included. Extra shunts have the effect of speeding the approach to steady-state, but reducing the steady-state level still further, improving the clamp in one respect but worsening it in another. For example, with g_{shunt} = 50 nS, the time to reach 99% of steady-state is decreased to 25.9 ms, but the steady-state is reduced to only 0.63 mV. Of course, if there were some way of approximately esti-

mating the shunt, then the decrease in the steady-state level could be compensated for, using a bigger command step. This suggests that, for a given series resistance, it might be possible to achieve nearer to the desired somatic responses with sharp electrode recording than with tight-seal whole-cell recording.

Dendritic voltage responses to a somatic step command are illustrated in Paper III for the CA1 pyramidal cell model.

DISCUSSION

The solution

General features

Following Rall (2), Bluman and Tuckwell (4), Evans et al. (5), and Paper I (1), separation of variables solutions have been derived for the voltage transients and clamp currents in a branching passive neurone cable model with the soma voltage clamped. The responses can be expressed as an infinite series of exponentially decaying terms. The time constants τ_n are obtained from the roots α_n of the recursive transcendental equation (Eq. 6) together with Eq. I.24. Because the different dendrites are uncoupled at the clamp point (e.g., Ref. 3), each α_n and therefore each τ_n originates from only one tree, and is constant throughout that tree. The amplitude terms are nonzero only in this source tree, and only if both the input and the recording site are also in the source tree or at the clamp point. (In some cases, where there is some symmetry in the morphology which would cause singularity clashes in the voltage recording solution, two or more roots from different trees may occur at the same value of α. They should be given separate indices, and then treated the same way as the other α_n values.) There are two basic cases, with the same time constants, from which the responses to arbitrary combinations of input currents and voltage commands can be built up, using the linearity of the system.

Case I: Unit point charge injected into a dendrite, soma clamped to zero

If the input site is a distance z_e along excitation segment e, the voltage response at x_r in recording segment r is

$$v_r(x_r, z_e, t) = \sum_{n=0}^{\infty} E_{n\,/\,(e)}\psi_{en}(z_e/\lambda_e)\psi_{rn}(x_r/\lambda_r)e^{-t/\tau_n} \qquad (59)$$

and the clamp current is

$$i_{\text{clamp}}(z_e/\lambda_e, t) = -\sum_{n=0}^{\infty} \alpha_n g_{\infty\,/\,(e)} E_{n\,/\,(e)}\psi_{en}(z_e/\lambda_e) \times [\sin \alpha_n L_{/\,(e)}]^{-1} e^{-t/\tau_n}, \qquad (60)$$

where λ_j is the space constant of segment j, $E_{n\,/\,(e)}$ is given in Eq. 14 and is independent of position within the source tree of α_n, and the two ψ functions are position-dependent spatial eigenfunctions, given in Eq. 10, one for the input site and one for the recording site. Note the symmetry between the two ψ functions in Eq. 59: exchanging input and recording sites will have no effect on the waveform, just as in the case of the simple voltage recording solution (Eq. I.56). $\mathcal{S}(e)$ is the stem segment of the tree containing the input (excitation) segment. $E_{n\,/\,(e)}$ is analogous to E_n in the voltage recording solution, but is simpler, depending only on terms from the source tree of α_n. The voltage is zero in noninput trees. Detaching noninput trees makes no difference to the clamp current at the soma or the voltage in the input tree. The ψ functions are also similar to those in the previous paper: the only difference being in the continuity factors: under voltage clamp $\kappa_{st} = 1$ for all the stem segments st. Following the convention in the Paper I, the indexing of the α_n terms starts from $n = 0$.

Case II: Unit voltage impulse command at the soma, no dendritic inputs

The voltage response is

$$v_r(x_r, t) = \sum_{n=0}^{\infty} \alpha_n g_{\infty\,/\,(r)} E_{n\,/\,(r)}\psi_{rn}(x_r/\lambda_r)[\sin \alpha_n L_{/\,(r)}]^{-1} e^{-t/\tau_n}. \qquad (61)$$

and the clamp current is

$$i_{\text{clamp}}(t) = -\sum_{n=0}^{\infty} (g_{\infty_{st}}\alpha_n)^2[\sin \alpha_n L_{st}]^{-2} E_{n_{st}} e^{-t/\tau_n}, \qquad (62)$$

where st is the stem segment of the source tree of α_n. The clamp currents into the individual trees and the soma sum linearly to give the total clamp current.

Other similarities with voltage recording solution

As is the case in Paper I, these solutions not only allow generation of waveforms, but also give the underlying component amplitudes and time constants. Most of the points in the discussion in the previous paper also hold for the voltage clamp case, e.g., the existence of closely spaced time constants when the geometry is complex, the insights afforded by explicit knowledge of the A_n and τ_n values, the representation of taper, lumped terms for smooth input functions, singularity clashes and the comparisons with compartmental models. It is worth adding that, because of the steeper attenuation of voltage transients under the clamp condition

than under simple voltage recording, finer compartmentalization is required to achieve a given agreement between compartmental model output and the analytical solutions. The increase in speed from using the analytical solution is therefore even greater with voltage clamp than with simple voltage recording.

Reciprocity relations

The voltage responses in Case I show the same symmetry between stimulation and recording sites as the voltage recording solution in Paper I. In addition, comparison of Eqs. 60 and 61 reveals that, for any dendritic location, the *voltage* response to a somatic *voltage* impulse is an upside-down version of the somatic clamp *current* following a *charge* impulse into the same dendritic site. A similar result for dendritic trees reducible to single equivalent cylinders is presented in Ref. 3. Because the system is linear, these reciprocity relations generalize to arbitrary input waveforms. Both symmetries could be exploited by compartmental modellers to reduce the number of simulations required to explore the effects of different input sites, and by experimenters as a further linearity test (in addition to checking for linear scaling of responses with inputs).

These *reciprocity relations* (see Discussions in Refs. 3 and 17) are a general feature of the impulse response (Green's function) of any linear system where the differential operator is self-adjoint (e.g., Ref. 18, Theorem 11, p. 816). They hold for any linear electrical network (e.g., Refs. 19 and 20), such as a compartmental model, and for any continuous passive cable tree (e.g., Ref. 21, p. 232).

Parameter dependence

The analytical solution clarifies the parameter dependencies of the responses of a cell under voltage clamp. All the time constants are proportional to C_m. In addition, the faster time constants are proportional to R_i and are independent of R_m. The slower time constants increase with both R_i and R_m. All impulse response amplitude terms are inversely proportional to C_m and are independent of R_m. The amplitudes of the voltage response to a synaptic impulse (Case I) are independent of R_i. The amplitudes of the corresponding clamp current, and of the voltage response to a voltage command impulse (Case II), are proportional to $1/R_iC_m$. The clamp current amplitudes for the voltage command are proportional to $1/R_i^2C_m$.

The only parts of the responses affected by R_m are the slower time constants: changes in R_m affect only the final decay of transients, hardly altering the peak. When fitting models to experimental clamp currents resulting from voltage *step* commands, the fast amplitudes of the target waveform constrain R_i and the fast time constants constrain C_m; the optimal R_m is then determined by the slower components. Fits which assume perfect voltage clamp should probably only be undertaken with double electrode recordings (from the same point). Given the likelihood of nontrivial series resistances with single electrode recordings, fitting clamp current transients while assuming perfect clamp may lead to misleading results.Uncertainty over the value of R_{ser} may worsen any fit nonuniqueness due to noisy data (e.g., Refs. 13 and 22 and Paper I).

Nonsomatic clamp point

Moving the clamp point would require new transcendental equations which would generate different time constants and amplitudes. It is easy to "re-organize" the representation of the cell as described above so that the given analytical solutions can be applied. Note that the solutions in this paper do not apply to the two-electrode voltage clamp where the voltage recording electrode is in a different part of the cell in relation to the current injection electrode.

Imperfect voltage clamp

No-shunt voltage recording and perfect voltage clamp are two extremes along a spectrum. The voltage recording α_n values are the roots of the recursive transcendental function (Eq. I.22), whereas the voltage clamp α_n values are the singularities. As argued above, for the transient parts of the solution, a series conductance between the clamp amplifier and the cell is equivalent to an extra shunt from the cell to earth. For the voltage transients following synaptic inputs, voltage recording with a shunt and imperfect voltage clamp to zero are therefore formally equivalent. The voltage solution for perfect voltage clamp to zero is in fact the limit of the voltage recording solution, as $g_{shunt} \rightarrow \infty$. With imperfect clamp, the clamp current is the negative of the somatic voltage, scaled by the series conductance.

The imperfect clamp solutions have the same reciprocity relations as those for perfect clamp. Parameter dependencies are similar to those for the voltage recording and perfect clamp solutions; in particular the early parts of transients are insensitive to R_m and g_{shunt}. As the series resistance increases, the coupling between the soma and the different dendritic trees becomes stronger and the clamp current into the whole cell deviates increasingly from the sum of the clamp currents into its isolated parts (see Example 2).

Interestingly, the slower time constants of a cell appear to show an approximately linear dependence on series resistance, for small series resistances. The effects of changes to the electrical or morphological parameters of a model on the intercept and slope of this relationship are discussed above. Intuitively, raising R_m or C_m, lowering R_i, or increasing diameters all worsen the effects of series resistance by bringing it into "effective electrical contact" with more membrane capacitance. Thus the effects of a given series resistance will be extremely model-dependent: the distortions caused to the responses will be worse for cells with a large "effective capacitance." This issue is explored further in Paper III.

When the series resistance is high (above about 50 MΩ), the series conductance (less than about 20 nS) will enter the

range of shunt conductances often experienced with sharp electrode recording (e.g., Ref. 13). Clamp current waveforms recorded with high series resistances will therefore bear more resemblance to inverted PSPs recorded with sharp electrodes than to the actual synaptic currents, particularly if there has already been some filtering by dendritic cables.

Whole-cell recording versus sharp electrode recording

Whole-cell recording is commonly assumed to be "superior" to sharp electrode recording. In order to temper this complacency, it is interesting to compare voltage clamp with a whole-cell pipette and with a sharp electrode *of the same series resistance*. The total conductance to zero is higher for the sharp electrode, and therefore voltage clamping is "better" than with whole-cell recording in one respect: the time constants are nearer to those generated with perfect clamp, and therefore the *time courses* of the clamp currents and actual soma voltage are less distorted (see Example 2). Of course, not all the axial current at the soma flows into the amplifier: a proportion is lost via the shunt. Naturally there are many other considerations when deciding which technique is most suitable for a given purpose.

Overview

The analytical solutions presented in Paper I and in this paper complement existing methods for generating transients in passive neurone models with arbitrary geometry. They also offer fresh insights, such as the symmetry between stimulation and recording sites in many situations, the underlying similarities between imperfect voltage clamp and voltage recording, and the parameter dependencies of the responses. Combined cable and series resistance effects will be considered in more detail in Paper III.

The techniques used, i.e., the construction of a recursive transcendental function to generate eigenvalues, and then the use of complex analysis to derive amplitude terms, are sufficiently powerful to be taken further: in future papers analogous solutions for models with nonuniform electrical parameters and extra *dendritic* shunts will be presented.

SUMMARY AND CONCLUSIONS

1) The simple voltage recording solutions in the previous paper are extended to give the responses of an arbitrarily branching passive neurone model under perfect somatic voltage clamp, both to current inputs and to voltage commands. As before, the solutions are obtained by separation of variables and are infinite series of exponentially decaying components.

2) The voltage clamp boundary condition effectively uncouples and isolates the dendritic trees originating from the clamp point. Each tree has its own transcendental function, the roots of which are eigenvalues in the exponential series. Each tree therefore generates its own set of time constants and spatial eigenfunctions, which, excepting coincidences, do not exist in the other trees. For a fixed clamp point, the time constants of a dendritic tree are independent of the stimulating and recording positions within that tree.

3) The *roots* of the voltage clamp transcendental equations of all the dendritic trees taken together are also the *singularities* of the voltage recording transcendental equation. The cell as a whole can therefore generate one voltage clamp time constant between every pair of voltage recording time constants.

4) Two fundamental kinds of input are considered: a unit point charge into a dendritic segment with the soma clamped to zero, and a unit somatic voltage impulse in the absence of any dendritic inputs. The amplitude terms can be obtained by complex residues or from the limit of the voltage recording solution as the shunt becomes infinite. Each depends only on the tree from which its particular eigenvalue originated.

5) The total clamp current required to impose a voltage command on a cell is the linear sum of the clamp currents required for the isolated individual dendritic trees and soma (but this relationship breaks down as soon as there is any significant series resistance).

6) The parameter dependencies of the solutions are similar to those of the voltage recording solution. In particular, the early parts of transients are relatively insensitive to changes in R_m and g_{shunt}.

7) The responses to a number of common current or voltage input functions are obtained analytically by convolution. Lumped amplitude terms are derived for the responses to inputs such as "alpha" function or exponentially decaying currents or voltage commands.

8) To obtain responses from a model with a nonsomatic clamp point, the real soma can be represented as a short cylindrical segment, and an extra soma of zero area can be introduced at the clamp point.

9) Expressions are derived for responses under imperfect voltage clamp. Clamping to zero is equivalent to voltage recording with an extra somatic shunt equal to the series conductance. The clamp current is an upside-down replica of the somatic voltage. The dendritic voltage response to a somatic voltage command is the negative of the somatic clamp current in response to a current input of the same waveform into the same dendritic site.

10) The slower time constants show an approximately linear dependence on series resistance for small series resistances. The larger the effective capacitance of a cell, the worse the effects of a given series resistance. Depending on the size, morphology, and electrical parameters of the cell, series resistances in the range used experimentally may cause serious attenuation and smoothing both of synaptic clamp currents and the voltage actually imposed on the soma.

11) As with the voltage recording solution, the analytic solutions for voltage clamp transients complement existing simulation methods, and offer additional insights into the composition and parameter dependencies of response waveforms.

APPENDICES

Appendix 1: Derivation of amplitude terms using complex residues

We follow closely Appendix 1 of the previous paper, with differences peculiar to the voltage clamp case highlighted.

Case I: Clamp to zero with synaptic input: $V_{com} = 0$, and unit dendritic point charge

We let $G_r(X_r, Z_e, t)$ be the voltage response at X_r to a unit charge impulse at Z_e in segment e, and as before, denote its Laplace transform by $\bar{G}_r$ (Eq. I.57). The Laplace transform of the system of equations describing the model is the same as Eqs. I.58–I.63 in Paper I, except that the somatic (clamp point) boundary condition (Eq. I.61) is replaced with

$$\bar{G}_s(Z_e, p) \equiv \bar{G}_{st}(0, Z_e, p) = 0. \tag{63}$$

We again have the definitions of $\bar{\mu}_p$, and $\bar{\kappa}_j$ (see Eqs. I.64 and I.66) in the previous paper), and use the same representation scheme for $\bar{G}_j$ (see Eqs. I.67-I.72). See Paper I, Fig. 9 for zoning of the dendritic trees.

Note that in noninput trees

$$\bar{G}_j = 0, \tag{64}$$

since the clamp boundary condition Eq. 63 forces $\bar{A}_s = 0$. Also, for the soma-input segment "mainline" chain's stem segment st,

$$\bar{A}_{st} = \bar{A}_s = 0. \tag{65}$$

We follow Appendix 1 of the previous paper, Eqs. I.73-I.77, for the determination of the $\bar{A}_c$, and $\bar{B}_c$ terms. Equations 64 and I.68–I.72, I.74, I.76, I.77, and 65 can be used to evaluate $\bar{G}_r(X_r, Z_e, p)$ over the entire dendritic tree.

Using the relationships (Eq. I.88) in the previous paper, and the transcendental equation (Eq. 6), it can be seen that $\bar{\kappa}_{st}$ also has simple poles at $q = i\alpha_n$, where st is the stem segment of the dendritic tree producing α_n. As in the voltage recording derivation, using the relationships (Eqs. I.73-I.77), it may be shown that $\bar{G}_r$ given in each of the expressions (Eqs. I.68-I.72), has poles at $q = i\alpha_n$. We note that near the poles the $\bar{B}_{st}$ term (Eq. I.77) comes to dominate $\bar{G}_r$ in all zones of the dendritic tree where $\bar{G}_r$ is nonzero. As can be seen from Eq. I.76, all other β_c terms contain an uncancelled $(\cosh qL_{st} + \bar{\mu}_{st}\sinh qL_{st})$ factor, which tends to zero near the poles. We define

$$h(p) = \frac{\bar{\kappa}_e\bar{\kappa}_r}{\bar{\kappa}_{st}^2 q}[\cosh q(L_e - Z_e) + \bar{\mu}_e \sinh q(L_e - Z_e)] \times [\cosh q(L_r - Z_r) + \bar{\mu}_r \sinh q(L_r - X_r)] \tag{66}$$

when $r \neq st$ and

$$h(p) = \frac{\bar{\kappa}_e[\cosh q(L_e - Z_e) + \bar{\mu}_e \sinh q(L_e - Z_e)]\sinh qX_{st}}{\bar{\kappa}_{st} q \sinh qL_{st}} \tag{67}$$

when $r = st$, with

$$k(p) = g_{\infty_{st}}(\bar{\kappa}_{st}\sinh qL_{st})^{-1} = g_{\infty_{st}}[\coth qL_{st} + \bar{\mu}_{st}]. \tag{68}$$

By evaluating the residues at the simple poles $p = -1/\tau_n$, as in Eq. I.83, we have

$$A_{n_{er}}^{vq} = \frac{h(p)}{k'(p)}. \tag{69}$$

Differentiating Eq. 68 with respect to p gives

$$k'(p) = \frac{\tau_m}{2q} g_{\infty_{st}}\left\{L_{st}(1 - \coth^2 qL_{st}) + \left\langle \frac{d\bar{\mu}_{st}}{dq} \right\rangle\right\}. \tag{70}$$

The recursive expansion (Eq. I.86) can be used on the term in angle brackets (□), and the substitutions (Eq. I.88), and the transcendental equation (Eq. 6) can be used with these expressions for $h(p)$, and $k'(p)$ to give $A_{n_{er}}^{vq}$ in Eq. 16.

Case II: Unit voltage impulse command: $V_{com} = \delta(t)$, no dendritic inputs

Now let $G_r(X_r, t)$ be the response to a somatic *voltage* impulse. The Laplace transform of the clamp point boundary condition (Eq. 1) is now

$$\bar{G}_s(0, p) \equiv \bar{G}_{st}(0, 0, p) = 1. \tag{71}$$

$\bar{G}_j$ is now given by Eq. I.67 over the entire dendritic tree. (All the $\bar{B}_j$ terms are zero.) It therefore follows that

$$\bar{A}_s = 1. \tag{72}$$

If $k(p)$ is as in Eq. 68, then

$$h(p) = g_{\infty_{st}} \frac{\bar{\kappa}_r}{\bar{\kappa}_{st}} \frac{[\cosh q(L_r - Z_r) + \bar{\mu}_r \sinh q(L_r - Z_r)]}{\sinh qL_{st}}. \tag{73}$$

This can be used together with Eqs. 70 and I.88 to derive $A_{n_{er}}^{vv}$ in Eq. 22.

Appendix 2. Amplitude terms for imperfect clamp unit impulse voltage command

Let $G_r(X_r, t)$ again be defined to be the response to a somatic *voltage* impulse. The Laplace transform of Eq. 38 with $V_{com}(t) = \delta(t)$ is

$$g_{ser} = g_s^* \bar{G}_s[1 + \epsilon^* \tau_m p] - \sum_{st \in stems} g_{\infty_{st}} \left.\frac{d\bar{G}_{st}(X_{st})}{dX_{st}}\right|_{X_{st}=0}. \tag{74}$$

With no input charges into the dendrites, $\bar{G}_j$ is given by Eq. I.67. Substituting this into (74) and applying $p = (q^2 - 1)/\tau_m$, gives

$$\bar{A}_s = g_{ser}\left\{ g_s^*[1 + \epsilon^*(q^2 - 1)] + q \sum_{st \in stems} g_{\infty_{st}} \bar{\kappa}_{st}[\sinh qL_{st} + \bar{\mu}_{st}\cosh qL_{st}] \right\}^{-1}. \quad (75)$$

Let $k(p)$ be defined as in Eq. I.82 and

$$h(p) = g_{ser} q^{-1} \bar{\kappa}_r \times [\cosh q(L_r - X_r) + \bar{\mu}_r \sinh q(L_r - X_r)]. \quad (76)$$

Then, following Eq. I.83, the amplitude terms in Eq. 41 can be derived from

$$A_{n_r}^{vv} = h(p)/k'(p), \qquad \text{at } q = i\alpha_n, \quad (77)$$

using $k'(p)$ in Eq. I.87, and with g_s^* and ϵ^* in E_n (Eq. I.34).

Appendix 3. Responses to sinusoidally varying inputs

Solutions

As discussed in Refs. 3 and 23 (Chapter 13), the cable equation for the A.C. steady state is the same as the Laplace transformed cable Eq. I.58b, but with the Laplace transform variable p replaced by $i\omega$, where $\omega = 2\pi f$ is the angular frequency. The A.C. steady-state (or frequency domain) responses can then be obtained directly from the unit responses $\bar{G}_j$ in the Laplace domain.

For an A.C. current $\tilde{I}$ injected at Z_e, the boundary condition is the same as Eq. I.63 with the right-hand side multiplied by $\tilde{I}$ (compare with Eq. B1 in Ref. 3): therefore the voltage response is $\bar{G}_j\tilde{I}$, with $\bar{G}_j$ as defined in Appendix 1 of Paper I.

For an A.C. voltage command $\tilde{V}_{com}$, with perfect clamp, the boundary condition is the same as Eq. 71 with the right hand side multiplied by $\tilde{V}_{com}$, so the voltage response is given by Eq. I.67 with $\bar{A}_s = \tilde{V}_{com}$. Likewise, in the case of imperfect clamp, the somatic boundary condition is given by Eq. 74 with the left-hand side multiplied by $\tilde{V}_{com}$, and so the voltage response is given by Eqs. I.67 and 75 with $\bar{A}_s$ multiplied by $\tilde{V}_{com}$.

A.C. clamp currents can be obtained using the Laplace transform of Eq. 18:

$$\bar{I}_{clamp} = -g_{\infty_{\mathcal{S}(e)}}(\partial \bar{V}_{\mathcal{S}(e)}/\partial X_{\mathcal{S}(e)})|_{X_{\mathcal{S}(e)}=0}, \quad (78)$$

where $\mathcal{S}(e)$ is the stem segment of the input site.

Implementations

In general, an A.C. response is a complex number $Me^{i\Phi}$, with a modulus (amplitude) M and a phase angle Φ. Rall and Segev (3) explain in their Appendix A how to calculate these quantities explicitly, for a single equivalent cylinder. Because a passive dendritic tree is a linear system, as a sine wave is propagated down the cables, the amplitude becomes attenuated and the phase becomes delayed, but no change in frequency occurs. Using their Eqs. A1–A5, recursive versions of their Eqs. A6–A10 can be derived for arbitrary geometries, to deal with the $\bar{\kappa}$ and $\bar{\mu}$ terms in the expressions for $\bar{G}_j$. However, the algebra is ugly, and it is probably simpler to do the calculations directly using complex arithmetic. There are several studies including derivations or descriptions of similar Laplace or Frequency domain solutions and algorithms (e.g., see Refs. 21, 24–32).

Frequency-dependent attenuation

Define $A_{ij}(\omega) = V_{ii}(\omega)/V_{ij}(\omega)$ to be the voltage attenuation at angular frequency ω between points i and j on the dendritic tree, where V_{ij} is the voltage at j in response to an input at i and V_{ii} is the voltage at i. Interestingly, if j lies on a direct path between i and k, then

$$A_{ik} = A_{ij}A_{jk}, \quad (79)$$

(21, 33). This is easily shown from the continuity of the Laplace transform solution: for clarity omit the somatic shunt and represent the soma as a short cylinder, and split any recording segment at the recording site (it is simple to extend the proof to cases with shunts and nonuniform electrical parameters). Treat the injection site as a "virtual" soma of negligible size. Then, from Eq. I.67,

$$A_{ij} = 1/\bar{\kappa}_j = \prod_{c \in chain_{ij}} (\cosh qL_c + \bar{\mu}_c \sinh qL_c), \quad (80)$$

where $chain_{ij}$ is the set of segments in a direct line from i to j, inclusive. Likewise,

$$A_{ik} = 1/\bar{\kappa}_k = \prod_{c \in chain_{ik}} (\cosh qL_c + \bar{\mu}_c \sinh qL_c). \quad (81)$$

Move the stimulation site to j, and change the representation of the cell so that the virtual soma is now at j. With the new representation, A_{jk} is given by

$$A_{jk} = 1/\bar{\kappa}_k = \prod_{c \in chain_{jk}} (\cosh qL_c + \bar{\mu}_c \sinh qL_c). \quad (82)$$

Equation 79 follows immediately from Eqs. 80–82.

The same relationship holds for steady-state attenuations, and for each amplitude term in the time domain, as can be seen from inspection of Eqs. I.33 and 16, for example. However, in general Eq. 79 does not hold for *peak* voltages, because most transient signals are composed of a number of different frequency components which suffer differential attenuation.

G.Major would like to thank Dave Attwell for helpful comments about reciprocity. We are grateful to Ken Stratford, Nelson Spruston, and Mike Häusser for helpful discussions and criticisms, and Alan Larkman for indispensable support and advice. We thank the Wellcome Trust for financial support (see Paper I).

REFERENCES

1. Major, G., J. D. Evans, and J. J. B. Jack. 1993. Solutions for transients in arbitrarily branching cables: I. Voltage recording with a somatic shunt. *Biophys J.* 65:423–449.
2. Rall, W. 1969. Time constants and electrotonic length of membrane

cylinders and neurons. *Biophys. J.* 9:1483–1508.

3. Rall, W., and I. Segev. 1985. Space-clamp problems when voltage clamping branched neurons with intracellular microelectrodes. *In* Voltage and Patch Clamping with Microelectrodes. T. G. Smith, Jr., H. Lecar, S. J. Redman, and P. Gage, editors. American Physiological Society, Bethesda, MD. 191–215.
4. Bluman, G. W., and H. C. Tuckwell. 1987. Techniques for obtaining analytical solutions for Rall's model neuron. *J. Neurosci. Meth.* 20: 151–166.
5. Evans, J. D., G. C. Kember, and G. Major. 1992. Techniques for obtaining analytical solutions to the multi-cylinder somatic shunt cable model for passive neurones. *Biophys J.* 63:350–365.
6. Major, G. 1993. Solutions for transients in arbitrarily branching cables: III. Voltage clamp problems. *Biophys. J.* 65:469–491.
7. Durand, D. 1984. The somatic shunt cable model for neurons. *Biophys. J.* 46:645–653.
8. Kawato, M. 1984. Cable properties of a neuron model with non-uniform membrane resistivity. *J. Theor. Biol.* 111:149–169.
9. Jackson, M. B. 1992. Cable analysis with the whole-cell patch clamp. Theory and experiment. *Biophys. J.* 61:756–766.
10. Spruston, N., D. B. Jaffe, S. H. Williams, and D. Johnston. 1993. Voltage and space clamp errors associated with the measurement of electrotonically remote synaptic events. *J. Neurophysiol.* In press.
11. Rall, W. 1959. Branching dendritic trees and motoneuron membrane resistivity. *Exp. Neurol.* 1:491–527.
12. Jonas, P., G. Major, and B. Sakmann. 1993. Quantal analysis of unitary EPSCs, at the mossy fibre synapse on CA3 pyrimidal cells of rat hippocampus. *J. Physiol.* In press.
13. Major, G. 1992. The Physiology, Morphology and Modelling of Cortical Pyramidal Neurones. D.Phil. thesis. Laboratory of Physiology, Oxford University. 275 pp.
14. Silver, R. A., S. F. Traynelis, and S. G. Cull-Candy. 1992. Rapid-time-course miniature and evoked excitatory currents at cerebellar synapses in situ. *Nature.* 355:163–166.
15. Clements, J. D. 1984. Ph.D. dissertation. Expt. Neurology Unit, John Curtin School of Medical Research, Australian National University, Canberra.
16. Sigworth, F. J. 1983. Electronic design of the patch clamp. *In* Single-channel recording. B. Sakmann, and E. Neher, editors. Plenum Press, New York. 3–35.
17. Abbott, L. F., E. Fahri, and S. Gutmann. 1991. The path integral for dendritic trees. *Biol. Cybern.* 66:49–60.
18. Rektorys, K. 1969. Survey of Applicable Mathematics. Iliffe, London. 1369 pp.
19. Irwin, J. D. 1987. Basic Engineering Circuit Analysis. MacMillan, New York. 612–615.
20. Smith, K. C. A., and R. E. Alley. 1992. Electrical Circuits—An Introduction. Cambridge University Press, Cambridge, UK. 546–547.
21. Koch, C., T. Poggio, and V. Torre. 1982. Retinal ganglion cells: a functional interpretation of dendritic morphology. *Phil. Trans. R. Soc. Lond. B.* 298:227–264.
22. Stratford, K. J., A. J. R. Mason, A. U. Larkman, G. Major, and J. J. B. Jack. 1989. The modelling of pyramidal neurones in the visual cortex. *In* The Computing Neurone. R. Durbin, C. Miall, and G. Mitchison, editors. Addison-Wesley, Reading, UK. 296–321.
23. Jack, J. J. B., D. Noble, and R. W. Tsien. 1975. Electric Current Flow in Excitable Cells. Oxford: Oxford University Press, Oxford, UK. 502 pp.
24. Norman, R. S. 1972. Cable theory for finite length dendritic cylinders with initial and boundary conditions. *Biophys. J.* 12:25–45.
25. Rall, W., and J. Rinzel. 1973. Branch input resistance and steady attenuation for input to one branch of a dendritic model neuron. *Biophys. J.* 13:648–688.
26. Rinzel, J., and W. Rall. 1974. Transient response in a dendritic neuron model for current injected at one branch. *Biophys. J.* 14:759–790.
27. Barrett, J. N., and W. E. Crill. 1974. Specific membrane properties of cat motoneurones. *J. Physiol.* 239:301–324.
28. Butz, E. G., and J. D. Cowan. 1974. Transient potentials in dendritic systems of arbitrary geometry. *Biophys. J.* 14:661–689.
29. Horwitz, B. 1981. An analytical method for investigating transient potentials in neurons with branching dendritic trees. *Biophys. J.* 36:155–192.
30. Koch, C., and T. Poggio. 1985. A simple algorithm for solving the cable equation in dendritic trees of arbitrary geometry. *J. Neurosci. Meth.* 12:303–315.
31. Turner, D. A. 1984. Segmental cable evaluation of somatic transients in hippocampal neurons (CA1, CA3, and dentate). *Biophys. J.* 46:73–84.
32. Holmes, W. R. 1986. A continuous cable method for determining the transient potential in passive dendritic trees of known geometry. *Biol. Cybern.* 55:115–124.
33. Brown, T. H., A. M. Zador, Z. F. Mainen, and B. J. Claiborne. 1992. Hebbian computations in hippocampal dendrites and spines. *In* Single Neuron Computation. T. McKenna, J. Davis, and S. F. Zornetzer, editors. Academic Press, San Diego, CA. 81–116.